Aalto University
School of Chemical
Engineering

Hamidreza Daghigh Shirazi

NOVEL APPROACHES FOR PRODUCING FILTER MEDIA

Master´s Programme in Chemical, Biochemical and Materials Engineering
Major in Functional Materials

Master's thesis for the degree of Master of Science in Technology submitted for inspection, Espoo, 31 July, 2020.

Supervisor: Professor Simo-Pekka Hannula

Instructors: M.Sc. Joonas Lehtonen
M.Sc. Mirva Mustakangas

Aalto University
School of Chemical
Engineering

Aalto University, P.O. BOX 11000, 00076
AALTO
www.aalto.fi

Abstract of master's thesis

Author: Hamidreza Daghigh Shirazi

Title of thesis: Novel approaches for producing filter media

Degree Programme: Chemical, Biochemical and Materials Engineering

Major: Functional Materials

Thesis supervisor: Professor Simo-Pekka Hannula

Thesis advisors: M.Sc. Joonas Lehtonen
M.Sc. Mirva Mustakangas

Date: 31.07.2020 **Number of pages:** 71 **Language:** English

Abstract

The performance of a filtering system is significantly influenced by the properties of the used filter medium. Various methods have been suggested in order to fabricate porous structures to be used as filter media. However, fabrication of the porous structures using these methods are often expensive, time-consuming and limited to certain ranges of porosities and pore sizes. Therefore, further research on developing these factors is still required.

The aim of this thesis was to develop porous filter media focusing on the controllable formation of pores in terms of total porosity and pore sizes. For this reason, metallic porous structures were developed using the space-holder sintering method and selective laser melting additive manufacturing technique, as new emerging fabrication methods. Results indicate the effectiveness of space-holder utilization in order to form pores in a variety of pore sizes and total porosities. Porosities of up to ~65% and pore sizes with different ranges of ca. 30 to 300 μm where achieved. Furthermore, the usefulness of this method for the fabrication of porous structures with a gradient of pore sizes has been confirmed. The applicability of selective laser melting has been evaluated by fabrication of multiple channels with various shapes, diameters and wall thicknesses. The optimum values and structures were determined. Analysis suggests that adjusting the design can effectively amend the practical limitations.

Keywords Filter media, porous materials, sintering, 3D-printing

Preface

This Master's thesis has been written in the Department of Chemistry and Materials Science at Aalto University during October 2019 – July 2020. The project was undertaken at the request of Outotec (Finland) Oy. I would like to express my gratitude to Mirva Mustakangas and Outotec (Finland) Oy for this interesting industry relevant topic and also financial support of the project. The worldwide Coronavirus pandemic had caused difficulties in conducting extensive research. Fortunately, Professor Simo-Pekka Hannula, Joonas Lehtonen, Mirva Mustakangas and Mika Salmi D.Sc. (Tech) have always been available and willing to respond to my inquiries. I am grateful to them for their unwavering guidance.

I would like to thank my supervisor, Professor Simo-Pekka Hannula, for giving me the invaluable opportunity of participating in the group of Advanced and Functional Materials, first as a research assistant and afterward, by trusting me with this project. I would also like to express my deepest gratitude to my instructor Joonas Lehtonen for his crucial role in the progress of this thesis, sharing his experience, being a great company and all the interesting endless conversations on literally every subject.

I would like to give special thanks to Dr. Mika Salmi for arranging and supporting the 3D-printing experiments in the School of Engineering. A special thank goes to Roy Björkstrand for his great contribution to 3D-printing experiments. I also want to thank Lassi Klemettinen for his significant help with performing the sintering experiments. I am grateful to Xuan Yang for her practical suggestions and being constantly supportive.

Finally, my warmest thanks go to my parents, who have always supported me with love and understanding through life.

Espoo, Finland
July 31, 2020

Contents

Abbreviations

ABP	Ammonium Bicarbonate Powder
ABS	Acrylonitrile Butadiene Styrene
CBN	Cubic Boron Nitride
CVD	Chemical Vapor Deposition
DIW	Direct Ink Writing
EBM	Electron Beam Melting
ECAS	Electric Current Assisted Sintering
ESF	Electro Sinter Forging
FDM	Fused Deposition Modeling
HIP	Hot Isostatic Pressing
HP	Hot Pressing
LCF	Laser Cladding Forming
LOM	Laminated Object Manufacturing
PBF	Powder Bed Fusion
PC	Polycarbonate
PECS	Pulsed Electric Current Assisted Sintering
PLA	Polylactic Acid
PMMA	Polymethylmethacrylate
PVA	Polyvinyl Alcohol
SEM	Scanning Electron Microscopy
SLA	Stereolithography
SLM	Selective Laser Melting
SLS	Selective Laser Sintering
SPS	Spark Plasma Sintering

1. Introduction

Filtration is an important process in many industrial and commercial activities, which would practically come to a halt without it. Filtration performance is largely dependent on the used filter medium. Filters are synthetic materials containing tiny pores for the fluid to pass through. In the filtration process, particles are physically strained at the surface as the fluid passes through the porous material in a pressure/vacuum-driven separation procedure. Despite the lack of a general system for classifying filters, they can be distinguished by their nominal pore dimensions, operating pressure and the type of filtered material.

An ideal filter material would be chemically resistant, physically durable, inexpensive and capable of permeating a high fluid flux without clogging. Therefore, the performance of filters is strongly affected by both the chemical and physical properties of the material, such as porosity, hydrophobicity and mechanical stability. A variety of polymer, ceramic, and metal-based materials have been proposed for use in filtration process. Early commercial polymeric materials, such as cellulose acetate, suffered from poor temperature resistance and a tendency to compact over time. Ceramic filters have also attracted attention because of their high pressure and temperature endurance, excellent chemical tolerance and hydrophilic surface that have low clogging tendencies. However, ceramic filters are fragile and even tiny undetectable cracks may affect the filtration process. Corrosion resistant metallic alloys, such as stainless steel, have become increasingly popular due to their processability and mechanical durability.

In recent years, additive manufacturing, also referred to as 3D-printing, has received considerable attention because it allows direct fabrication of complex shapes. Additive manufacturing technologies provide the possibility of building objects using pre-defined structures by sharing the same principle of incremental addition of an appropriate material in a layer-by-layer procedure. In the case of metallic materials, the deposition of metals has become feasible through the use of methods, such as the powder bed fusion method. Although most previous research has focused on

fabrication of near full density parts, less interest has been directed toward highly porous materials suitable for filtering applications.

Another common approach for fabricating metallic parts is to use a sintering process. In this process, metallic powders are compacted using thermal energy. New sintering techniques have been developed for achieving complex geometries or modifying process constraints. For instance, introducing joule heating and pressure can be used to shorten the process and reduce the sintering temperature. Typically, the presence of pores has been, however, considered to be a sintering defect and harmful in industrial products due to the deterioration of their functional properties. Nevertheless, highly porous materials would be advantageous for use as filters. Therefore, developing high-performance porous materials has remained a challenge. In order to overcome this challenge, this thesis develops porous materials by controllably applying pores in a dense solid matrix, known as the space-holder method.

1.1. Objectives

The aim of this thesis is to evaluate sintering methods and additive manufacturing techniques for future development of porous filter materials with high and controllable porosities. These methods will be characterized in terms of their porosity, pore sizes and microstructure. Their practicability in filter production is evaluated by developing filter materials using the identified methods to determine their advantages and limitations. This thesis focuses only on the filtering media and its fabrication processes. Fabrication of the whole final filter remains outside the scope of this thesis. In the present work, the fabricated porous materials are made of stainless steel on account of its desirable properties, such as excellent corrosion resistance and high strength.

1.2. Structure of the thesis

The remainder of this thesis is divided into seven chapters. Chapter 2 reviews and evaluates emerging sintering techniques for fabrication of porous materials. This is followed by describing the space-holder technique as an attractive method for forming the desired porosities. Chapter 3 elaborates different types of additive manufacturing

processes, focusing on their applicability as a means for filter media production. A review of the literature on the filter media is presented in Chapter 4, which assesses the various fabrication techniques for the three different types of polymeric, ceramic and metallic materials. Chapter 5 describes the experimental procedure for filter fabrication used in this work, using both the space-holder method and the powder bed fusion additive manufacturing technique. Chapter 6 reports the results of the experiments, including the fabrication processes and performed characterizations. Chapter 7 discusses the results obtained for the fabricated materials in terms of their physical properties, pore formation, microstructure and morphology. Finally, Chapter 8 concludes this thesis by summarizing the applicability of these results for additive manufacturing and sintering as well as describing directions for future research.

2. Sintering process

Sintering is an important process in the field of powder metallurgy, as well as ceramic industries. Its theoretical concepts are originated upon porous materials discrete organization. The contact between particles grow as the result of activation of thermal adhesion process, causing the particles to coalesce. The kinetics of sintering in a porous body is not only determined by the properties of the powder particles and the nature of their interactions, but also by macroscopic governing factors. These factors include externally applied forces, homogeneity of properties through the volume (such as density variation caused by preliminary pressing) and kinematic constraints (e.g. sample surface and furnace adhesion). [1]

2.1. Pressure-less sintering

Sintering happens at temperatures higher than half of the melting point. The system tends to reduce the surface free energy, and thus considered to be the process driving force. Therefore, the solid-vapor interface with higher free surface energy is replaced by solid-solid interfaces [2]. At this stage, bonding is followed by the formation of necks by either surface or bulk transport mechanisms, whereas atomic level diffusion occurs based on vacancies. Figure 1 schematically demonstrates the grain growth and densification as means of the total surface energy reduction [3].

The surface transport mechanism reduces the free surface energy by surface diffusion or evaporation condensation, while the necking happens and particles spacing remains the same without occurrence of densification. Conversely, volume and grain boundary diffusions along with plastic and viscous flow are the key factors for bulk transport mechanism, resulting in both necking and densification. [3]

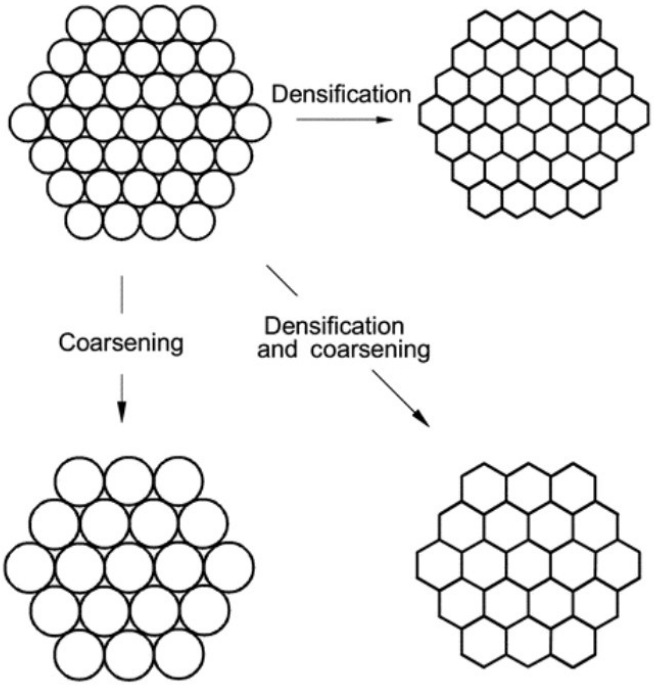

Figure 1. Schematic of phenomena happening in sintering process by the driving force of sintering [3].

2.2. Liquid phase sintering

Liquid phase sintering is consisted of a coexisting liquid and particulate solid at certain points of the sintering process. Two main ways of obtaining liquid phases are: 1) using mixed initial materials with dissimilar chemistries and 2) having two powders that their interaction during sintering causes a liquid phase. The liquid phase can be either formed by a eutectic reaction or melting of a constituent. Solubility of the solid in liquid can greatly affect the sintering rate and microstructure. Further, the solid/liquid interfacial energy and relative penetration of liquid in solid grain boundaries are notable factors. Process parameters are also influential, such as temperature, duration, particle size and atmosphere. [4]

Typically, the liquid wets the solid and also it has a level of solubility for it. As a result, the liquid acts on particles to remove pores and decrease the free surface energy. The classic process of liquid phase sintering involves three main steps to densify the

powders. Figure 2 demonstrates these stages. In the first stage, rearrangement occurs by heating the powders to form liquid phase at certain temperature, whereas initial densification rapidly begins by wetting liquid on particle surfaces due to capillary force. The minimization of the surface free energy eliminates porosity. The amount of liquid, powder size and solid solubility determine the level of densification. For instance, rearrangement of finer particles is usually more successful, and formation of sufficient liquid (~35 vol.%) may result in full density by a better rearrangement. On the other hand, inhibiting the rearrangement processes is possible by using irregularly shaped particles or high green densities, since the contact resulted by compression prevents the rearrangement. 2) *solution-reprecipitation*: although the rearrangement is kinetically fast and more noticeable, but the rearrangement densification slows down and the effects of concurrent solubility and diffusivity become more significant. This is noted as solution-reprecipitation stage. Since the smaller grains have a higher solubility, a concentration gradient in the liquid occurs due to the different solubilities. Materials are transferred from small grains to the larger ones (Ostwald ripening) and coarsening happens. Therefore, fewer but larger grains will be grown. In this step, the sample is also densified by allowing a tighter packing of the grains due to the diffusive transport and solid solubility. Finally, the solid-state stage, which is also active during the other stages, becomes dominant in the end. Since the solid skeleton is formed, densifying performs slowly and rearrangement is not possible. Nevertheless, diffusion continues the microstructural coarsening. Therefore, elongation of sintering time deteriorates the properties. [4,5]

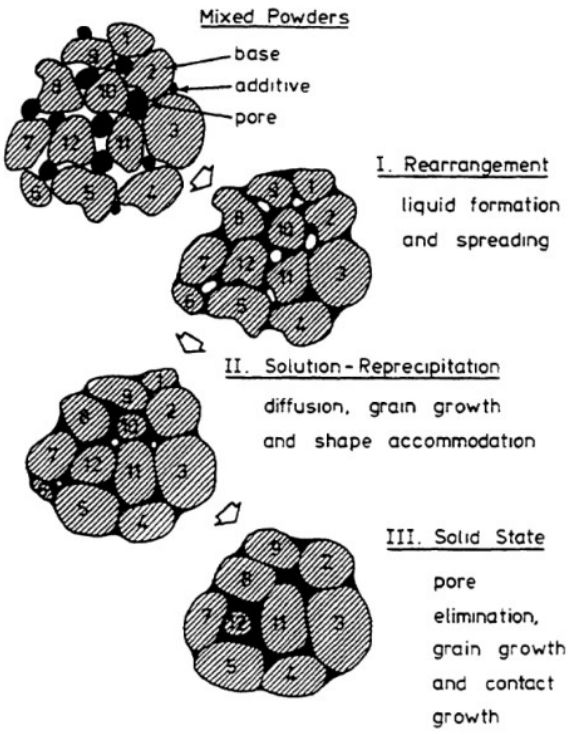

Figure 2. The stages of liquid phase sintering, including mixed powders and formation of liquid by heating [4].

Assembly of fibers/wires by sintering is a noteworthy approach to fabricate highly porous permeable metals with high strength and possibility of optimizing the microstructure and properties [6]. Metallic wires have good mechanical properties and are widely available. Fabrication of relatively tough highly porous material using liquid phase sintering of short stainless steel fibers is reported [6]. In this method, the fibers that were initially electroplated by copper are heated to sintering temperature. Then the liquid copper generates joints in fibers contact areas.

In the liquid phase sintering process, the sintering is expedited by fast atomic diffusion comparing to that of solid-state sintering. In addition, there is no need for external pressure since the capillary attraction leads to a rapid compact densification. Typically, the phase with higher melting point is also the harder one. This leads to fabrication of a two-phase composite with a ductile attribute. This feature can be regardless of the quantity dominance of the harder phase. On the other hand, the formation of

inappropriate amount of liquid during the sintering process may cause a shape distortion. As a result, selection of appropriate parameters becomes challenging. [4,5]

2.2.1. Pulsed electric current sintering (PECS)

Pulsed electric current sintering is an advanced technology, which is used to consolidate powders of a wide range of materials [7]. In this sintering technique, a combination of uniaxial compression and pulsed direct electric current is applied to sinter the sample at desired temperatures. The required temperature is achieved as electric current passes through the sample. It provides the heat using the Joule effect, without any external heating source. Therefore, it is classified as a resistance sintering technique. The distinct nature of heating in this process results in inhomogeneous distribution of heat through the powder particles, concentrating on particles contact areas that leads to an efficient sintering procedure [8,9].

The PECS process enables the possibility of fabrication of fine grain materials with near theoretical densities [10]. This prevention of grain growth is due to high heating rate, lower required sintering temperature, and shorter sintering duration. Therefore, PECS is not only a simpler method in comparison to the conventional ones, but also capable of accomplishing results that would have been near impossible by those techniques. Figure 3 schematically presents the PECS process.

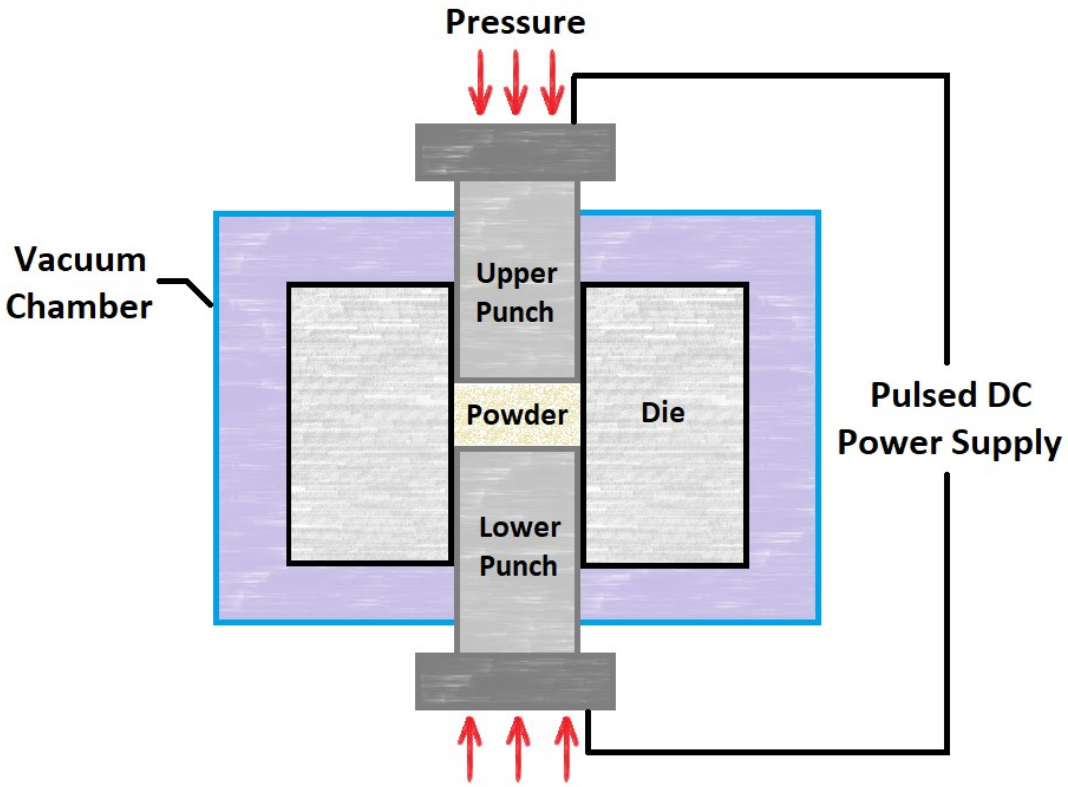

Figure 3. An illustration of the PECS process.

In this technique, shapes of sintered samples are however limited to symmetrical objects. It requires an expensive DC generator, and additionally, in the case of particle sizes less than 100 nm, significant gradient of temperature happens. This results in non-uniformity of microstructure. [11]

The feasibility of combining fast heating advantage of SPS and the aspects of conventional pressure-less sintering has been successfully investigated by coupling these two methods in a modified setup [12]. In this setup (Figure 4), common graphite mold and punches of SPS are substituted by a graphite crucible. The sample is placed on the heating element, and therefore, heat transfer is conducted from the bottom and radiation from the sides. The graphite crucible is place in between graphite plates to avoid the direct exposure of steel rams to high temperatures. Some recent attempts have focused on production of highly porous materials using either pressure-less [13] or conventional setup, and removal of inorganic salts, e.g. NaCl [14].

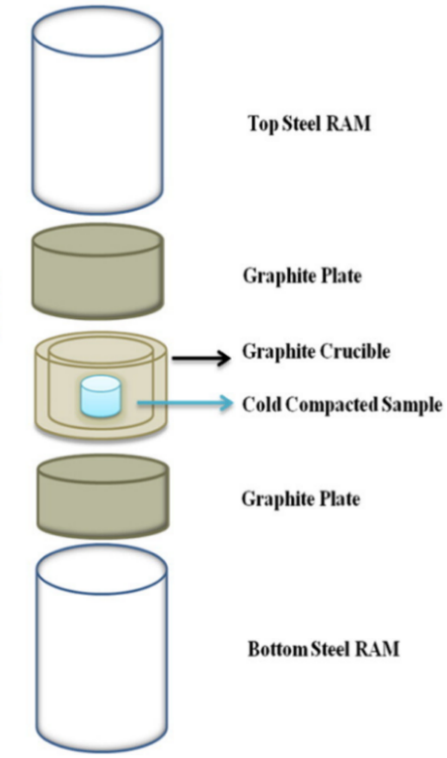

Figure 4. Schematic of a pressure-less SPS setup [12].

In general, the lower sintering temperature in SPS in comparison with conventional techniques, and short time of process (applying pressure, increasing temperature and holding) results in an excellent control over microstructure, and especially grain growth for nanomaterials [15]. Moreover, fabrication of composites is possible with different initial powders and homogenous final microstructure [11]. Apart from the privilege that quick heating provides, local pressure and plastic deformation of particles aids the possibility to achieve a high density [1]. Conversely, high porosities are also achievable using low pressures and temperatures along with a short holding time [1].

In comparison with hot pressing and conventional methods, absence of external heating, and consequently a high heating rate has shortened the sintering process to several minutes. While in those techniques, the process may take several hours and even days. The aforementioned features and high production rate can decrease the costs. [11]

2.2.2. Electro sinter forging (ESF)

Another innovative electric current assisted sintering technique is electro sinter forging (ESF). This method is a developed version of capacitor discharge sintering, which consists of a single short impulse of electric current along with pressure, allowing near complete consolidation of powder particles [16]. In this technique, an electrically conductive powder is sintered in a very short time (> 1 s), and reaches high density. The short electric current impulse takes place with a mechanical pulse. It is required to pre-apply pressure before the quick single pulse and optimize the specific energy input. The sintering can be performed in either solid or liquid phase. [17]

2.1. Electric current assisted sintering (ECAS)

Electric current has been utilized in various sintering techniques, in two categories of resistance sintering and electric discharge sintering. The history of exploiting electric currents to assist sintering goes back to early 20^{th} century. Nowadays, hot pressing and hot isostatic pressing are well-known ECAS technologies. Figure 5 shows the number of publications on the subject of electric current assisted sintering through the years. The increasing number of publications in this field demonstrates its attraction as rapid consolidation techniques. [9]

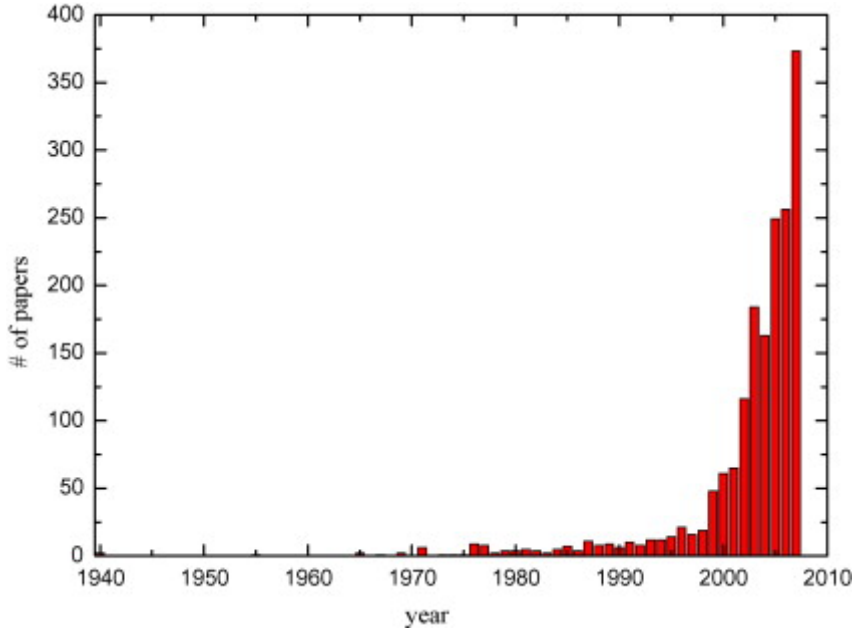

Figure 5. Number of electric current assisted sintering publications through the years [9].

Pressure assisted sintering technique is a category of sintering methods that have been widely used in hot pressing (HP) and hot isostatic pressing (HIP) techniques. The goal is mainly to achieve high densities which are not reachable using pressure-less sintering. Applying pressure provides the advantage of sintering at lower temperature. This prevents the grain growth, and thus improves the mechanical properties. [18]

In hot pressing, a uniaxial pressure is applied in a rigid die at high temperatures. In conventional hot pressing, there is merely applying of pressure and temperature using e.g. induction furnace. The heating can be provided by resistance, induction (rapid) or exothermic reactions (very rapid). The pressure is applied in the direction of vertical axis, however, a radial pressure exists against the lateral walls of the die. Addition of heat and pressure effectively results in pore-free materials. Figure 6 schematically illustrates the hot pressing process. [18,19]

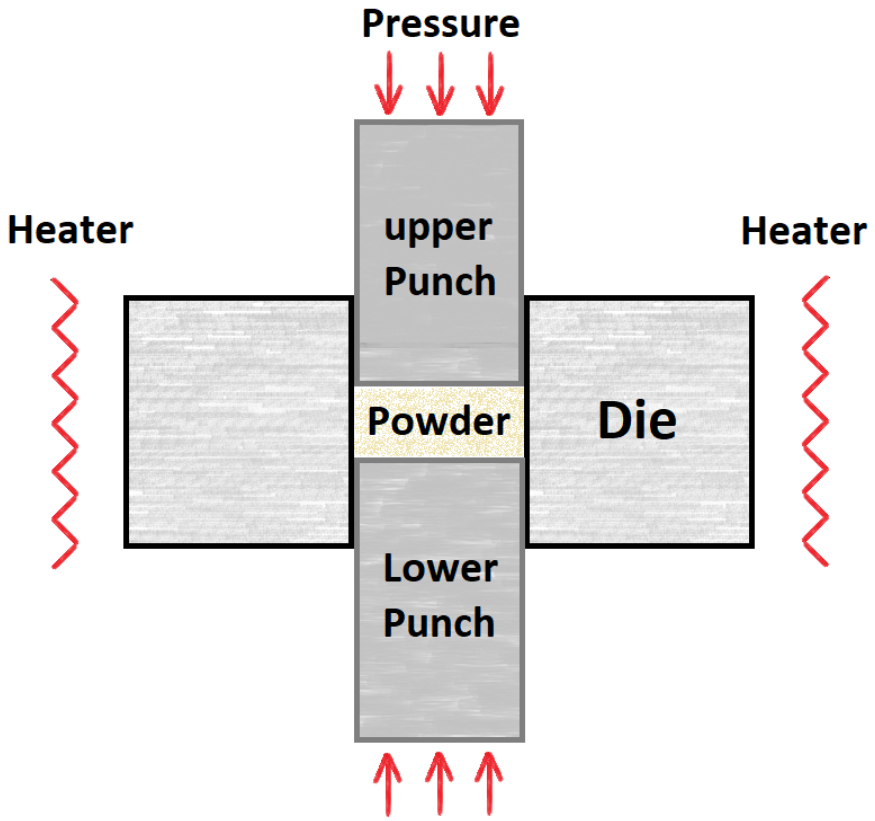

Figure 6. A schematic illustration of uniaxial hot pressing.

Hot isostatic pressing utilizes a hydrostatically applied gas pressure in a furnace to form fully dense materials. Pressures higher than PECS process is achievable and comparing to HP, the nature of applied pressure leads to a uniform densification in a sealed container that is initially evacuated from gases. The initial sintering process is carried out in vacuum, followed by pressurization in order to seal the residual pores. Figure 7 presents a schematic of the HIP process. [18,19]

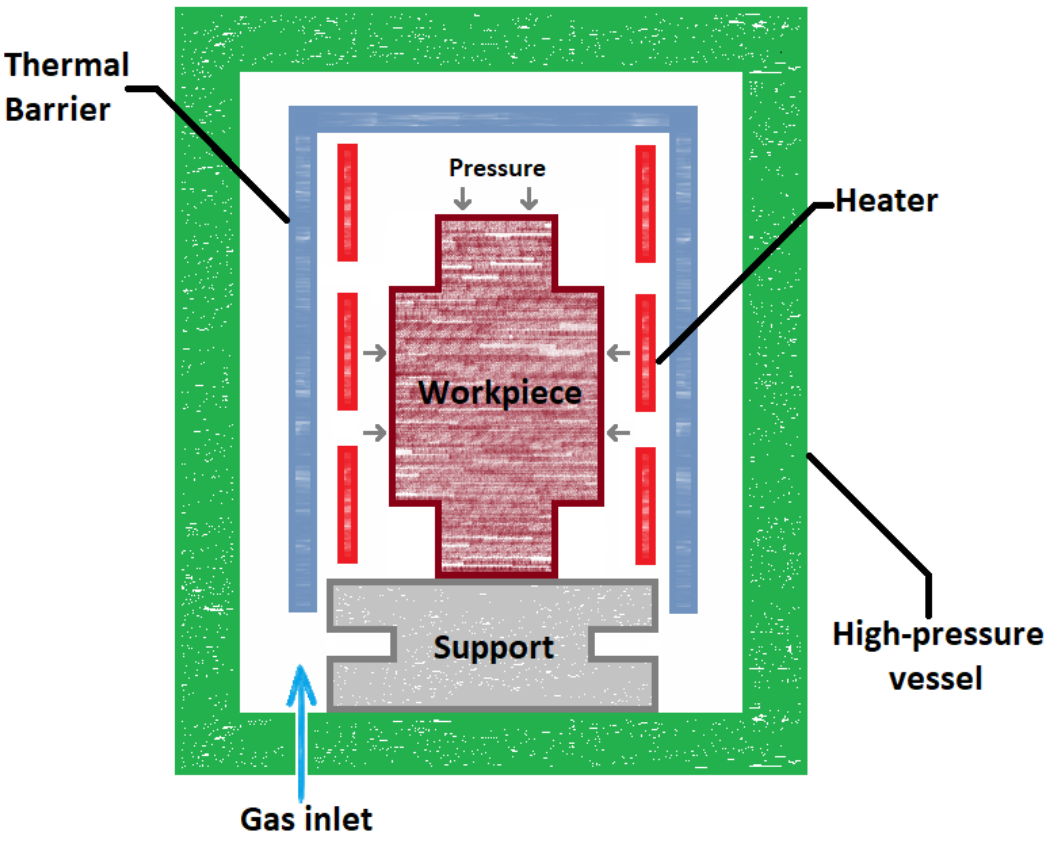

Figure 7. Schematic of HIP process.

3. Additive manufacturing

The technology of additive manufacturing has risen from the idea of discrete accumulation forming, so that complex 3-dimensional parts are controlled by CAD model/data and applied by the principle of material accumulating fabrication. Therefore, it is classified as a “bottom to up” material manufacturing method, in contrast to the traditional machining technology and material cutting. Omitting the multi-step forming processes makes this method a substantially short process, emphasizing the more complex shapes. The additive manufacturing technology emerged in late 1980s, and so far, various types of processes are developed, such as powder bed fusion, material extrusion and material jetting. The usage of these were soon found in various fields, including aerospace, electronics, automation and medical industry. [20-22]

The main difference between the additive manufacturing techniques is the used material and how the layers are deposited. The speed, cost, and resolution of the techniques also differ, e.g. the additive manufacturing of metals is typically expensive. [20,23]

3.1. Powder bed fusion

Powder bed fusion (PBF) includes several techniques, such as electron beam melting (EBM), selective laser sintering (SLS) and selective laser melting (SLM). The heating source, i.e. laser or electron beams, fuses the powder to build a layer. Then the excess of powder is removed. [20]

Fraunhofer institute proposed SLM first in 1995 and developed by MCP company in 2003 [24]. To this point, the commercially available equipment is developed by different companies, such as EOS, Concept Lase, and ILT companies. SLM is a precise technology that is used to form complex metal structures. SLM operation is run in an inert gas chamber, in which, a powder spreader supplies the metal powder and a high-power-density laser scans the surface. The laser melts the powder to fuse the metallic

powder. This continues layer-by-layer till the formation of designed bulk material by metallurgical bonding. Figure 8 demonstrates the schematic positioning of different parts in a SLM process. [24,25]

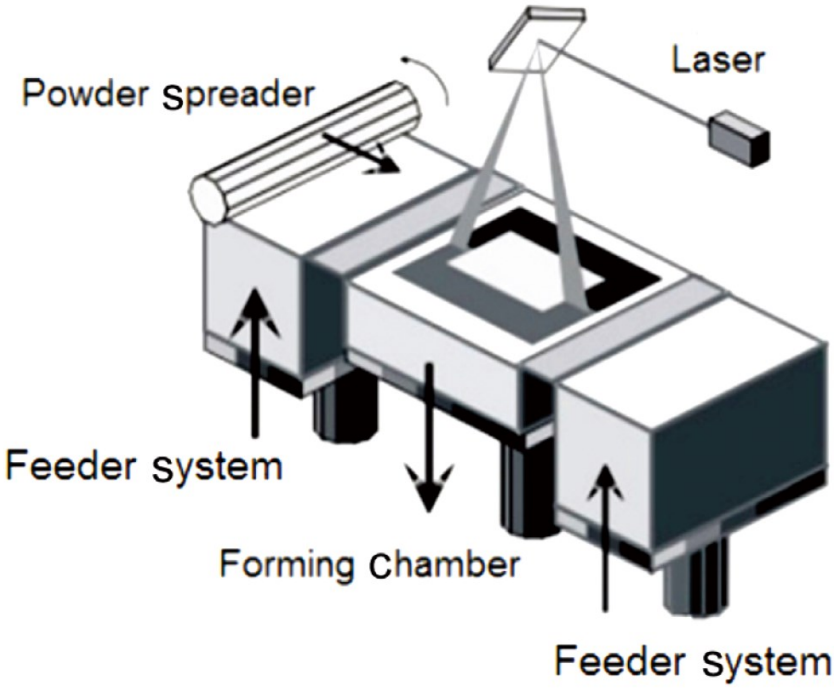

Figure 8. An illustration of SLM process [24].

Electron beam melting (EBM) operation is run under vacuum, in which a heating source of electron beam conducts the designed patterning on the metal powder, similar to SLM process. Therefore, the major differences between EBM and SLM are the heating source and chamber atmosphere. Due to higher energy of EBM (more than 10 times) and larger beam spot size, the forming speed is up to five times faster than that of SLM. On the other hand, the SLM equipment are cheaper, more technologically developed, and have higher precision because of the smaller laser beam spot size. [25]

In EBM and SLM processes, the preparation of metal powder is of an influential part of technology development. There are various expectations that should be met, such as small particle size, narrow size distribution, low oxygen content and high sphericity. Currently, the powders are commonly prepared by plasma atomization, plasma

spheroidization, vacuum induction-melting inert gas atomization, and also electrode induction-melting inert gas atomization. The metal powder variety is mostly limited to 316L, Ti6Al4V, CP-Ti, IN625, and CoCrMo. [24]

Fabrication of porous metallic materials by SLM/EBM are pursued in the form of crystal lattice and honeycomb structures. To produce porous structures by SLM, first a CAD model of a porous structure should be designed. The shape, size and distribution of pores are determined in this step. These parameters are limited by the resolution of the SLM system, which are governed by laser spot diameter, powder particle size, and particle morphology. During the process, the laser beam scans the powder except for the pore located regions. In the end, the remaining powder is removed from the porous structure. The powder size distribution is generally in the range of 10 - 100 μm, and consequently, limiting the pore diameter. The used powder is in the atomized form, which is an economical way of producing spherical particles. The spherical powder particles are desirable because they provide the possibility of high packing density and flowability. These features lead to reproducible rapid spreading of powder. [26]

3.1.1. Benefits and challenges

The possibility of producing materials to the size of 400 mm can be reached using many SLM machines. The used materials include stainless steel, copper, aluminum, titanium, tungsten, and cobalt chromium. It is reported that the 3D-printed samples may have up to ~50% higher yield than that of as-cast alloy. This is due the very fine microstructure of the samples prepared by SLM. [27]

Nevertheless, the number of processable materials is yet limited and process setting needs further development. For instance, in the case of Aluminum alloys, the challenges are due to high reflectivity, high thermal conductivity and light weight. [28]

Production of thin walls is a challenging process by SLM additive manufacturing. While the final quality is dependent on several factors, such as printing machine parameters, minimum printable plate thickness and structure design. It is suggested

that the minimum printable thickness is determined by the minimum plate thickness of the structure. Moreover, the resulting mechanical properties of the walls are largely affected by these parameters. For instance, a considerable reduction of the material ductility has been reported for decreasing the wall thickness from 1 mm to 0.5 mm in an additively manufactured stainless steel 316L. [29]

Similar to SLM, the energy source to provide the heat for sintering process in the selective laser sintering (SLS) technique is also provided by a laser beam. In this technique, the particles of e.g., polymers, are fused together without melting. [30]

3.2. Material extrusion

Material extrusion additive manufacturing, also trademarked as fused deposition modeling (FDM) is a common additive manufacturing method, in which a heated movable nozzle extrudes a spooled polymer. The nozzle moves on the surface, and as the bed adjusts the height, extruded material build the object layer-by-layer. These layers bond to each other by controlling the temperature or chemical bonding agents. Support are generated to hold the overhanging structures. The broad availability of materials in this technique includes polylactic acid (PLA), acrylonitrile butadiene styrene (ABS), Polycarbonate (PC), polyurethanes and nylon. Figure 9 illustrates the material extrusion additive manufacturing process. [31,32]

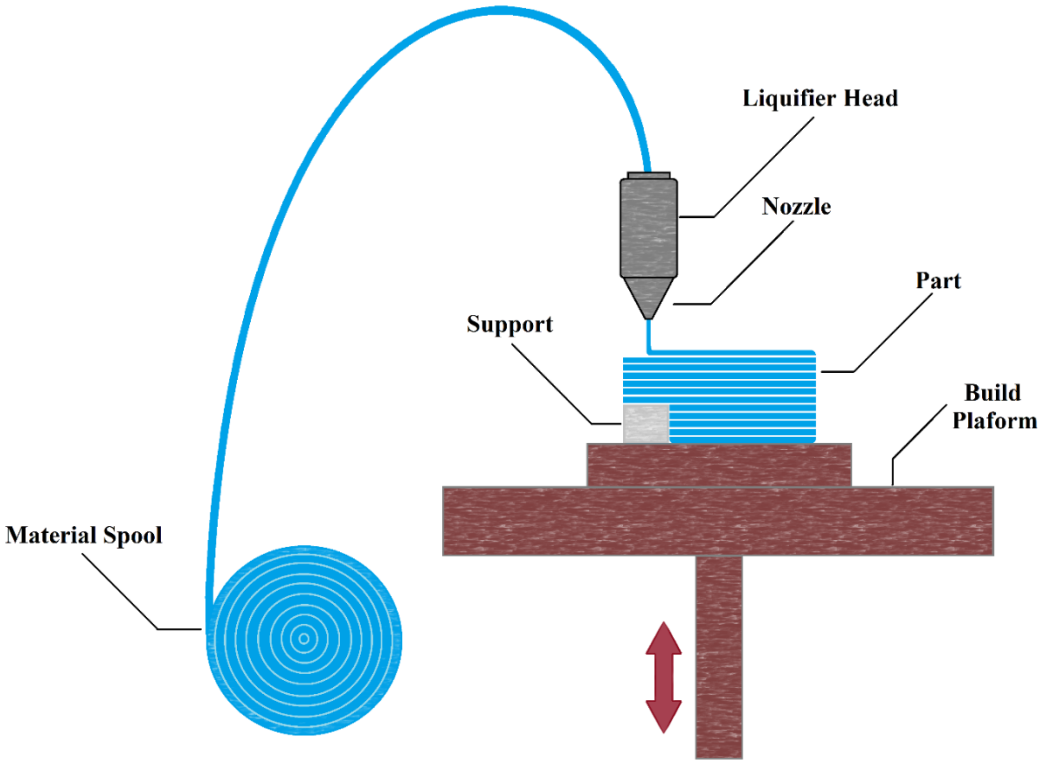

Figure 9. A schematic illustration of material extrusion additive manufacturing method.

Composite fabrication is possible by utilizing multiple extruders. The fabrication of composites is also possible using one extruder, in the case that adequate amount of base thermoplastic material is available to ensure the fusion [33]. One of the main challenges in material extrusion is the anisotropy of mechanical properties caused by the orientational building. This challenge arises from the anisotropic nature of additive manufacturing methods. In material extrusion, the anisotropy may cause a difference of multiple times in e.g. tensile test [34].

3.3. Material jetting

In the material jetting additive manufacturing technique, also known as inkjet 3D printing, parts are built by deposition of droplets of photopolymers and cured by ultraviolet exposure. In this method, several polymer resins can be simultaneously used [35]. The supports are printed using dissolvable materials and removed after the

process. Material jetting has been utilized to produce various type of structures, including honeycomb structure and scaffolds for tissue engineering [36,37]. Figure 10 schematically shows the material jetting process.

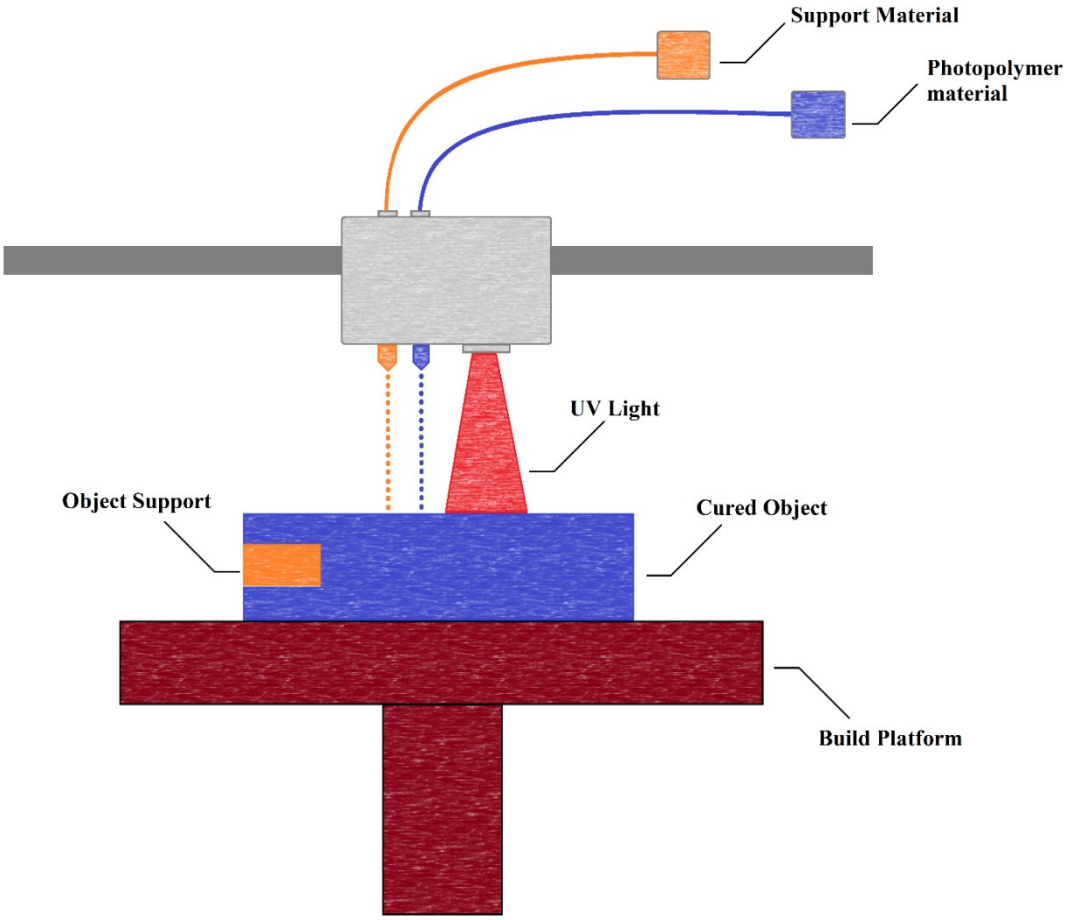

Figure 10. An illustration of material jetting process.

The printing orientation in material jetting method has a significant role in surface quality, dimensional accuracy and strength. Furthermore, the mechanical properties of the cured photopolymers may deteriorate and cause brittleness. Also, a minimum wall thickness of 0.4 mm is required to guarantee successful fabrication. [35]

3.4. Other additive manufacturing methods

In the Vat polymerization additive manufacturing technique, a vat of liquid resin photopolymer is utilized. Layers of the resin are cured using a light source that selectively performs the polymerization process by following a pre-defined geometry. The configuration in this technology may be either upright style or an inverse configuration. In the upright configuration, also known as stereolithography (SLA), the build plate submerges into the resin vat, the polymerization is performed between the build plate and resin surface, and then the build plate lowers for a new resin layer to be formed. Alternatively, in the inverse configuration, the build plate is pulled upward from a tray of resin. In the building process of each layer, a leveling blade runs across the resin surface and physically levels the surface. The resins usually possess a high viscosity, which makes it challenging to form a layer with uniform thickness in upright configuration. One way to overcome this issue is the usage of a leveling blade to physically flatten the surface. An advantage of inverse configuration is the shorter process since the geometry and thickness of the layers are mechanically limited by solid surfaces before the polymerization. The produced part in bottom-up configuration can be larger than the vat. [25]

Another common additive manufacturing technique is binder jetting. In the binder jetting technique, alternating layers of powder material and an adhesive are deposited to form a 3D geometry. The adhesion is accomplished by a liquid binder. [20]

In the sheet lamination method, ultrasonic welding is used to combine metal sheets. This process requires low energy and temperature. Laminated object manufacturing is another sheet lamination technology that produces 3D objects by alternating use of the main material and adhesive. [20]

4. Filters media: a review of literature

By the definition, A filter medium is defined as “any material that under the operating conditions of the filter, is permeable to one or more components of a mixture, solution or suspension, and is impermeable to the remaining components” [38]. The remained components may be solid particles, colloidal materials or ionic species. Any material with a porous structure can serve a filter medium, regardless of the sizes of its pores. It should be strong, resistant to corrosion and abrasion, flexible, and have the possibility to contain the desired porosity. These requirements reduce the number of options for the media, however, a variety of candidates exist, from inorganic materials, such as metals, ceramics and minerals, and either natural or synthetic organic materials.

In this review, various techniques for fabricating porous media are presented, focusing on the applicability of emerging sintering techniques and additive manufacturing methods. For this means, each section discusses the following three categories of materials: metals, ceramics and polymers.

4.1. Metallic filters

Production of a durable metallic filter would directly influence its implementation. The production of porous metals is possible through different approaches, such as injection of gas into the molten metals [39], powder metallurgy processes (solid-state formation of foams) [40], usage of foaming agents in liquid metallurgy [41] and baking/sintering of metal powder aqueous slurry [42]. The final properties of the foam are dependent on the used materials, the carried-out process and its parameters. Currently, filters made of stainless steel and aluminum are in industrial use, in which the minimum pore sizes can be as low as 2 μm [38]. As a comparison, stainless steel foams show superior strength, modulus and absorption of energy comparing to aluminum, as these characteristics are proportional to that of the dense material [39,43]. Stainless steel foams also have excellent corrosion resistance [44].

One of the most important characteristics of a porous material is its porosity, i.e. the fraction of pores in the material. Successful fabrication of highly porous materials with porosities of up to 97% are reported [45]. Some of the common manufacturing processes of porous metals are presented in Table 1 to provide an overview of the fabrication methods, porosities, pore sizes, cost and used materials.

Table 1. Common methods for fabrication of porous metals. [46]

Method	**Cost**	**Cell-type**	**Pore size (mm)**	**Maximum Porosity**	**Materials**
Space-holder	Low	Open	0.05-1.5	85%	Al, Steel, Cu, Ti, Ni
Casting (using a template)	Medium	Open	1-5	85%	Al, Steel, Cu, Mg, Ni-Cr
Metal deposition on cellular preform	High	Open	0.01-0.3	98%	Ni, Ti
Melt gas injection	Low	Closed	5-20	97%	Al, Mg
Expansion of entrapped gas	Medium/ high	Closed	0.01-0.3	86%	Ti

In the metal gas injection method, gas bubbles in the melted aluminum lead to the porous structure [47], while in the entrapped gas expansion, the formed pores by the hot isostatic pressing are elongated using hot rolling to increase porosity. In the casting using a template, different materials can be used in a negative image of the desirable template foam. The metal deposition method consists of chemical vapor deposition or electrodeposition on a template [45]. In the space-holder method, the desired porosity is generated by removal of a space-holder material and sintering the metal. In this section, space-holder method is elaborated, and materials, porosities and pore sizes are reviewed.

Powder metallurgy, and utilization of space-holder method in particular, has drawn extensive attentions toward making stainless steel foams, due to its significant advantages [48-50]. Figure 11 demonstrates the different stages of space-holder method. In this method, space-holder materials with desirable shape and size are selected with precision. Carbamide [48,51], ammonium bicarbonate [52], NaCl [53], cenosphere [49] and saccharose [54,55] are some of the used space-holder materials. The total porosity can be controlled by adjusting the volume fraction of space-holder material. The space-holder, metallic particles and a binder are mixed and compressed in mold to form a green compact. The space-holder particles are removed to provide the pores, and the green compact is then sintered at high temperatures to obtain final porous material.

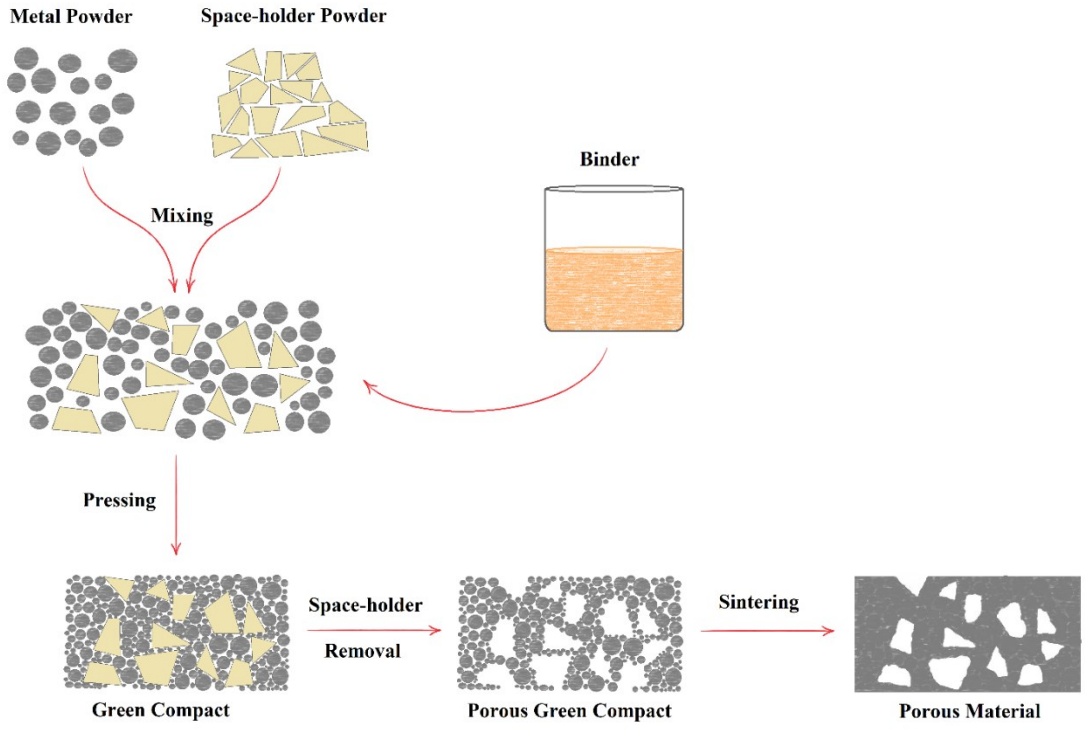

Figure 11. A schematic illustration of space-holder method in order to fabricate porous materials.

In a research by Becoz and Oktay [48], usage of differently shaped carbamide space-holder (spherical and angular) resulted in a successful fabrication of steel foams with

a maximum porosity of 65%. After compressing the mixture of metal powder, space-holder and a binder (polyvinyl alcohol) to achieve the green compact, water leaching was used at room temperature for space-holder removal. Then, the sintering was performed at 1200 ℃ in a controlled hydrogen atmosphere.

Fabrication of materials with higher porosities have been also tried using carbamide space-holder particles. Porosities of up to 70% using 750–1000 μm space-holder size is reported by water leeching. The addition of boron was also examined as a liquid phase additive, and successfully removed the unwanted micro-porosities and improved the mechanical properties of the porous material. [50]

Nishiyabu *et al*. successfully produced micro-sized porous structures by combination of metal powder hot press molding and the space-holder method. polymethylmethacrylate (PMMA) was used as the space-holder material and stainless steel 316L as the matrix. A complete decomposition of PMMA requires heating to 500℃. The importance of sintering temperature and the size of metal and space-holder particles were investigated. A considerably high shrinkage of 15-20% was reported for porosities of even less than 50%. A higher sintering temperature resulted in both lower porosity and specific water flow, addressing the resistance of a fluid to flow through the sintered porous material. Furthermore, highest ratio of space-holder to metal particle sizes minimized the shrinkage. It was concluded that spherical metal particle size and temperature are two significantly influential parameters. [57]

In a recent research by Hangai *et al*. [58], multilayered aluminum foams with functionally graded materials were fabricated. The fabrication was performed using sintering dissolution process, in which, NaCl with the size of 300-425 μm was utilized as the space-holder. The limitation of this method is the size of NaCl particles, which is much larger than metal particles to ensure effective removal in dissolution process in a flowing water. The sintering was performed by PECS and an average porosity of 70% has been successfully achieved.

Combination of liquid phase sintering and space-holder method was shown to synergize their advantages [50]. For this means, control over pore morphology, distribution, size, and porosity is combined with higher integrity in metal matrix, avoiding unwanted micro pores.

4.2. Ceramic filters

Ceramics have attracted considerable attention for filtering applications due to the possibility to have dispersed pores and the ceramics intrinsic properties, including heat, corrosion, wear and erosion resistance [58]. As filters, porous ceramics possess a high pressure and temperature endurance, excellent chemical tolerance and hydrophilic surfaces that have low clogging tendencies. These features enable the possibility of aggressive cleaning. However, the high capital cost of ceramic filters has hindered the application of these systems [59].

Aluminum oxide (Al_2O_3, Alumina), titanium oxide (TiO_2, Titania), zirconium dioxide (ZrO_2, Zirconia) and silicon dioxide (SiO_2, Silica) have been widely used as porous filter media [38,60]. Alumina is the most commonly used material as ceramic filters because of its high abrasion and wear resistance, thermal stability, abundancy and low cost [61]. Titania is also a popular filter material due to its excellent chemical resistance, in both acidic and basic environments [60]. Zirconia is a very stable material that can be used in oxidizing atmosphere at temperatures higher than 2000 °C and is a suitable candidate for filtering applications as a result of its stability in alkaline solutions [60,61]. Silica suffers from hydrothermal instability. Water molecules can be physically absorbed to the Si-OH groups in the presence of heat and moisture. Despite the wide usage of silica filters in gas separation systems (e.g. H_2 and CO_2), it cannot be considered as a candidate for the fluid filtration [62].

The early filters were made of a single material, however, the current developed ones have a composite structure. In this case, a thin layer of a material containing micropores contributes to high quality of filtration, while a microporous substrate provides the required strength. The combination of these layers may be done e.g. by lamination or coating the thin layer on the strong substrate. These composite structures can be found in different types of materials, but much attention has been directed toward inorganic and especially ceramic materials. [38,60]

Ceramics with porous structures can be produced by different techniques, such as solid-state sintering, sol-gel process, burning a sponge polymer out of the ceramic slurry and gel casting processes. These conventional fabrication methods are problematic in terms of requiring toxic solvents, residual polymer particles removal

difficulty, little control over pore shapes, insufficiency of pores interconnections, being time consuming and poor repeatability. 3D-printing techniques provide the possibility of fast, flexible, low-cost and direct fabrication of porous ceramics. The 3D-printing of porous ceramic objects is done by selective laser sintering, selective laser melting, fused deposition modeling and stereolithography. The ceramic powder and its characteristics, such as shape and particle size distribution, directly affect the final structure and its properties. For instance, fine ceramic particles promote printability by producing thin layers, resulting in low surface roughness. In contrast, large particles have lower surface to volume ratio, and therefore, the bonding of particles by the binder would be improved. [63,64]

The SLA process of ceramics can be addressed by use of a ceramic suspension system. Various ceramic materials, including alumina and zirconia, have been successfully prepared using an ultraviolet laser to solidify the part in a photo-polymerization process. [65]

In a recent work, highly porous TiO_2 has been successfully produced by material extrusion additive manufacturing method [66]. The novelty of this work was the addition of zinc, as the frothing agent, to the mixture of TiO_2 powder and polyvinyl alcohol (PVA) binder. Zinc and PVA reacted and generated bubbles, resulting in a porosity of 65% and pores with an average size of 180 μm.

A novel processing route toward producing open-porous cellular structures has been developed by a capillary suspension-based ink [67]. In this method, alumina particles were mixed with a secondary phase (binder) and printed in a direct ink writing (DIW) process, in an approach similar to material extrusion, in which the part is built by depositing small amounts of paste or ink. The samples are then thermally debinded and sintered. A porosity of 45-60% and pore sizes smaller than 6 μm were reported. Table 2 presents several 3D-printed porous materials with various porosities and pore sizes.

Table 2. The achieved porosities and pore sizes of several 3D-printed ceramic materials.

Material	Method	Porosity	Pore Size
Alumina	Direct ink writing [67]	45-60%	< 6 μm
Alumina	DIW + foam templating [68]	88-93%	5-20 μm
Alumina/Camphene	Material extrusion [69]	67-77%	> 150 μm
TiO_2	Material extrusion [66]	65%	> 180 μm
Silica, Calcium carbonate	A self-developed 3D printer with laser-aided gelling [70]	34%	800 μm
Silica, Zinc oxide	Binder Jetting [71]	29%	300 μm

4.3. Polymeric filters

The filters can typically be divided into woven (obtained by weaving) and non-woven categories. Although the non-woven filters usually possess a higher permeability and no yarn slippage problem, the woven filters are being more extensively used due to their lower price, low pressure drop and recent improvement on their temperature resistance. [72]

Polymeric filters can also be produced by solvent casting (or phase inversion). In this method, the basic polymer is dissolved in a solvent, and addition of another solvent leads to precipitation of the polymer. The final filter is produced by either evaporation of the solvent or by extrusion, which can result in hollow fibers. [38]

For the case of woven fabrics, despite the importance of their pattern and how they are fabricated, many properties depend on the nature of the used materials. The fabric properties of different polymers are presented in Table 3.

Table 3. The properties of polymeric filter media fabrics. [38]

	PTFE	**Nylon**	**PVC**	**PP**	**Acrylic**	**Aramid**	**Polyester**
Tensile strength (Relative, PTFE=1)	1	2.9-5	1.7	2.9-4.6	1.4-2.9	3.8-15.4	2.8-4.8
Maximum elongation at break (%)	15	20	40	35	42	20	14
Maximum service temperature (°C)	280	120	100	100	140	260	140
Maximum continuous service temperature (°C)	260	110	90	90	135	220	135
Chemical resistance							
Strong acids	✓✓✓	dissolves	✓✓✓	✓✓✓	✓✓	✓	✓✓
Weak acids	✓✓✓	✓	✓✓✓	✓✓✓	✓✓✓	✓✓	✓✓✓
Strong alkalis	✓✓✓	✓✓	✓✓✓	✓✓	✓✓	✓✓	dissolves
Weak alkalis	✓✓✓	✓✓✓	✓✓✓	✓✓✓	✓✓	✓✓	✓

4.4. Challenges and opportunities

Table 4 evaluates the promising filter materials and their respective production methods. In this evaluation, 3D-printing and modern sintering techniques are of special interest. In order to draw a comparison, the possibility of producing interconnecting open pores, controllable pore sizes, process simplicity and intrinsic properties of the materials are taken into account.

Table 4. An evaluation of potential filter materials and their respective production methods.

Material		method	Notes
Metals	Stainless steel	PBF [73-75]	• Dense matrix with very good corrosion resistance • Resolution limitation • Porosity gradient have resulted in high flow rates
		Space-holder [50]	• Pore size controllability • Various porosities • Simple and repeatable
	Ti	Space-holder [76]	• Interconnecting pores • High porosities
	Ti–6Al–4V	EBM [77]	• Lattice structure fabrication • High porosity • Very good mechanical properties
Ceramics	Al_2O_3	Space-holder [78]	• Corn starch as space-holder • Porosity of ~ 40% and pore sizes of ~ 3 μm. • Promising corrosion resistance and mechanical properties
	TiO_2	Direct foaming [66]	• Very high porosities • Interconnectivity should be examined
	Silica-bonded SiC	Sintering + sacrificial template [79]	• Controllable porosity • Fine pores • Simple sintering process
	Si_3N_4	Freeze-Drying [80]	• Unidirectional aligned channels • High sintering temperature • Micron and submicron pores • Undesirable closed- pores in small pore sizes

		Space-holder [81]	• Unidirectional channels • Nylon as pore forming agent • Orienting the pores by extrusion • Limited porosity
Polymers	Polypropylene (PP)	SLS [82]	• Limitation on scaled- down structures
	PTFE	SLS [83]	• Porosity of > 80% • High water flux • Shows the importance of design improvement
	Nylon	FDM/ PBF [84]	• Increased particle deposition comparing to commercial filters
	Natural polylactic acid (PLA)	FDM [85]	• Higher strength, water flux, reverse solute flux and fouling resistances compared to ABS and PP

5. Experimental procedure

This chapter presents the procedures to fabricate porous materials using the space-holder method and the powder bed fusion additive manufacturing technique. Section 5.1 presents the used raw materials. Section 5.2 describes the performed experiments in order to fabricate the desirable porosity. The utilized characterization techniques to study the powders and fabricated samples are presented in Section 5.3.

5.1. Raw materials

5.1.1. Space-holder method

The final porous materials were made of stainless steel 316L powders (Osprey metals ltd), and Ammonium hydrogen bicarbonate particles (noted as ABP, Riedel-de Haën) were used as the space-holder. Stainless steel 316L powder was used as received. ABP powder was sieved to the sizes of 32-63 μm, 63-90 μm, 90-150 μm, and 150-300 μm.

Polyvinyl alcohol (PVA, Mowiol® 10-98, Aldrich) was used as the binder to strengthen the green compact. The binder was applied as aqueous solution with concentration of 5wt.%. A release agent (20-8185-002, Buehler) was used to lubricate and ease the removal green compact from the mold.

5.1.2. Powder bed fusion

The used powder in this method was also stainless steel 316L (EOS GmbH). It was chosen similarly to the space-holder method to provide the possibility of comparison of properties. However, the powders have had different providers.

Designing the geometries was performed using SolidWorks CAD software to the Stereolithography (STL) format in order to be realized by the machine. The designed geometries are shown in Figure 12. The channel diameters in Figure 12a have varying

sizes of 100, 150, 200, 300, 400, and 500 µm with a depth of 5 mm. The wall thicknesses have the sizes of 100, 200, 300, 400 and 500 µm. Figure 12b and Figure 12c show the designed geometry of channels with a channel size gradient. In these cases, channels with circle cross-section (noted as conical, Figure 12b) and square cross section (noted as pyramidal, Figure 12c) are designed. The channels have a narrow end of 300 µ and broad end of either 400 or 500 µm. The wall thicknesses are 300, 350, and 400 µm.

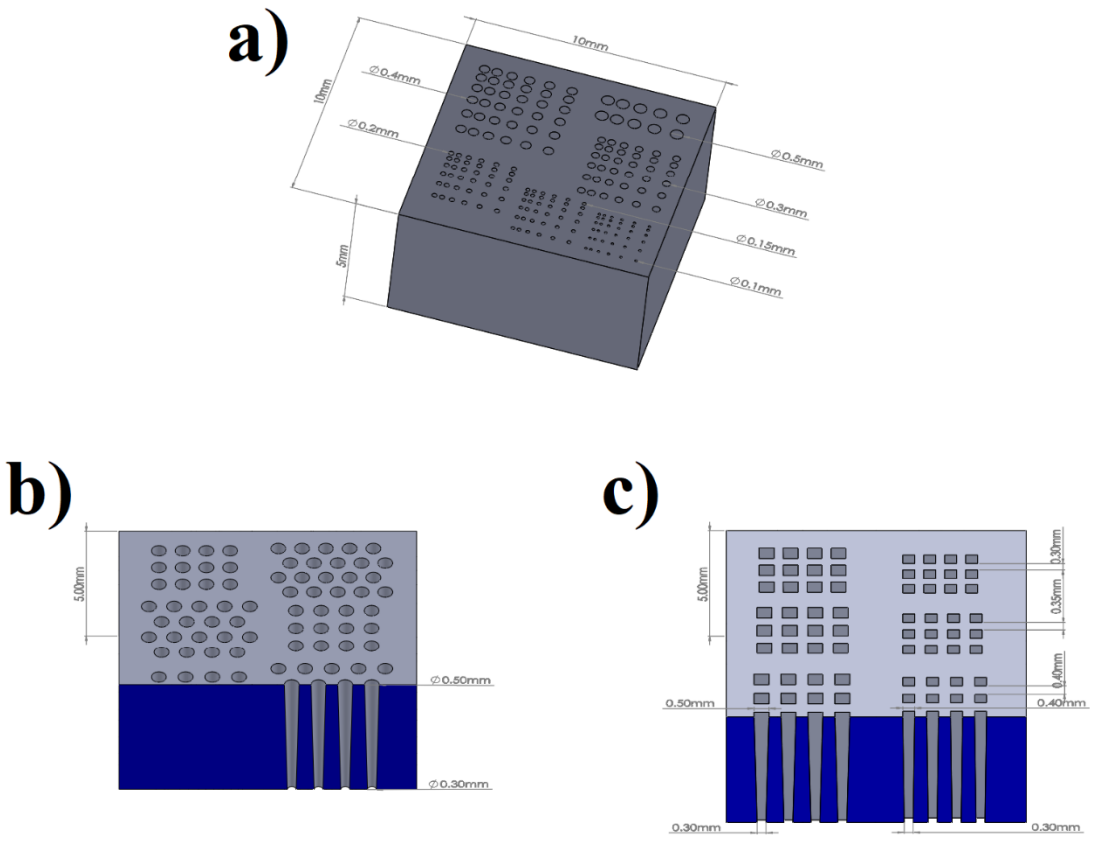

Figure 12. The designed geometries containing a) cylindrical, b) conical and c) pyramidal channels.

5.2. Fabrication

5.2.1. Space-holder utilization

The stainless steel 316L and ammonium bicarbonate powder (ABP) powders were mixed in a shaker mixer (Turbula Type T2C) for 30 minutes and 60 rpm. Table 5 shows the initial amounts of powder batches in fabrication process. The powder mixtures have ABP volume fractions of 0%, 50%, 60%, 70% and 80% with ABP nominal particle size of 150-300 µm. Also, mixtures with fixed 70% volume fractions of ABP and altering ABP particle size of 32-63 µm, 63-90 µm and 90-150 µm were prepared. Furthermore, formation of a gradient of pore sizes was sought in a layer-by-layer insertion of 63-90 µm, 90-150 µm and 150-300 µm ABP particles with a 70% fixed ABP volume fraction.

Table 5. Samples and information on their respective components.

Sample No.	Space-holder size	Space-holder Volume fraction	Amount of Stainless Steel 316L	Amount of ABP
1	-	-	3.1416 g	-
2	150-300 µm	50%	1.5708 g	0.1964 g
3		60%	1.2666 g	0.3737 g
4		70%	0.9424 g	0.4360 g
5		80%	0.6283 g	0.4983 g
6	90-150 µm	70%	0.9424 g	0.4360 g
7	63-90 µm			
8	32-63 µm			
9	Gradient of Samples 4, 6 and 7	70%	2.1206 g	0.981

The prepared PVA solution was added as the binder with an amount of 2 wt.% of the whole mixture. A cylindrical steel mold with a diameter of 1 cm was used for the compression of the powder mixture. The mold was first lubricated using the releasing agent solution, left for 30 seconds and then dried using a dust-free tissue. The mixture was placed in the mold and two punches were used for applying the pressure. A pressure of 500 MPa was applied for 30 seconds using a hydraulic press (HP20 AA/AR, Compac Hydraulik A/S). Figure 13a shows a general view of the hydraulic press machine. The space-holder particles were then removed at 200℃ for 1 hour. The removal of the space-holder was monitored by measuring the weight of the sample. Next, the samples were placed in a controlled atmosphere tube furnace (Lenton LTF16/450) in order to sinter the samples (Figure 13b).

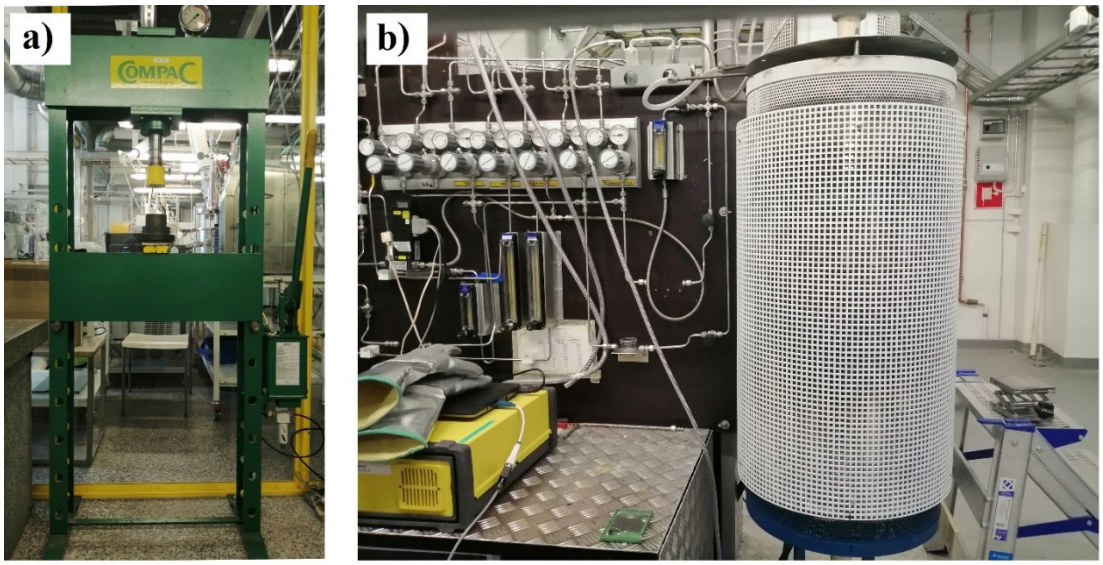

Figure 13. A general view of a) the pressing machine and b) the tube furnace equipment.

A nitrogen gas flow with flow rate of 200 mL/min was used to prevent oxidation at high temperatures. The samples were first heated with a heating rate of 2 ℃/min to 400 ℃ and kept for 1 hour in order to remove the binder. Afterwards, it was heated to 1200 ℃ with heating rate of 4.5 ℃/min and sintered for 1 hour at the temperature of 1200 ℃. Figure 14 shows the temperature profile of the sintering process.

Finally, the feasibility of producing a size gradient of pore structures was investigated. In this case, layers of powders were prepared with ABP particle sizes of 63-90 µm, 90-150 µm, and 150-300 µm and 70% volume fraction of ABP powder.

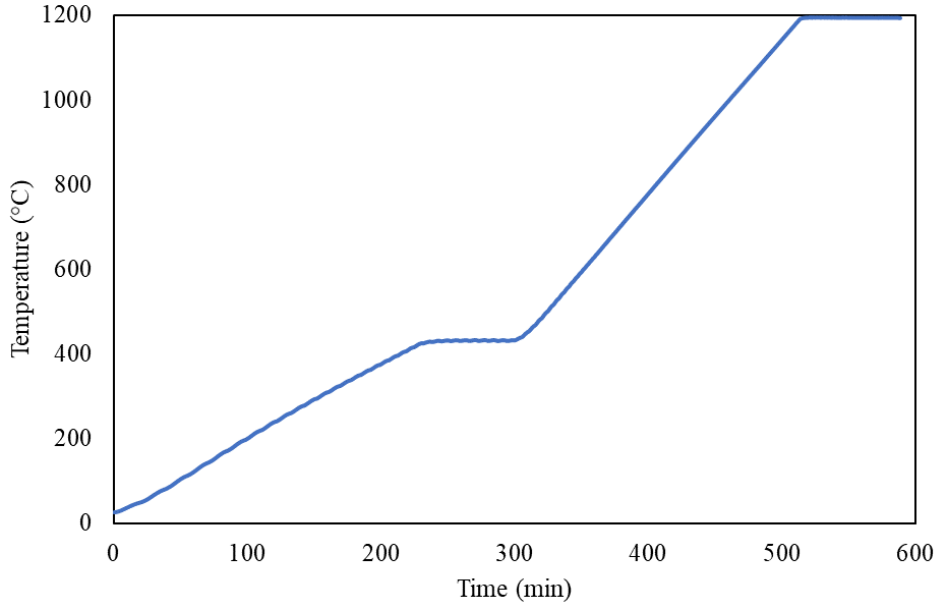

Figure 14. Temperature profile of the sintering process, corresponding to sample 2 sintering experiment.

5.2.2. End-use 3D-printing

Powder bed fusion was utilized to prepare porous structures containing various sized-channels. The best resolution for fabrication of channels was pursued. The printing was done by EOS M290 metal 3D-printer (Figure 15). This machine is capable to construct a volume of 250 × 250 × 325 mm, scan speed of up to 7.0 m/s, and focus diameter of 100 µm. It uses a 400 W Yb-fiber laser type in an inert gas-controlled atmosphere of Argon in order to prevent oxidation.

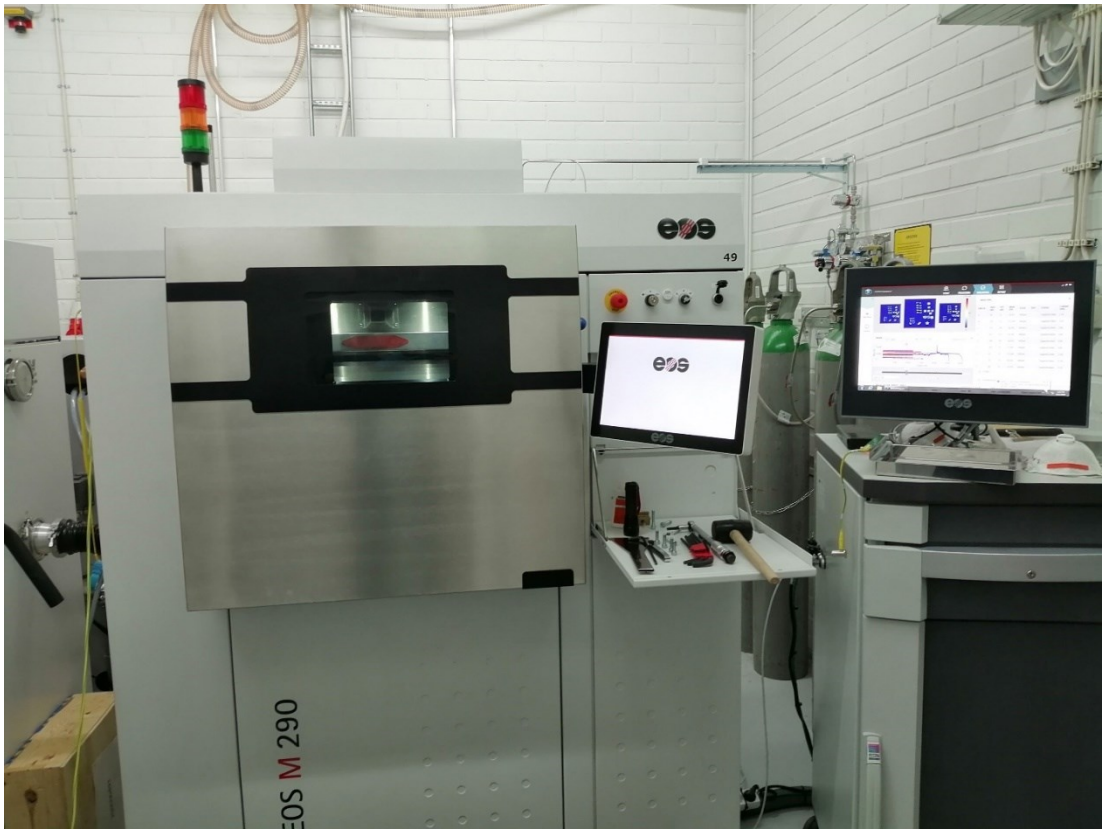

Figure 15. A general view of the EOS M290 metal 3D-printer.

The process requires the indication of different sets of parameters, including infill, upskin and contour, where stripes width and their overlap, laser power, speed, and hatch distance (the separation distance between two consecutive laser beams) are selected. Figure 16 schematically shows an illustration of hatch spacing. The stripes themselves are consisted of a series of hatches. Each layer of powder has a thickness of 20 μm. In infill section, parameters referring to the inner part of the sample are selected. Stripe width of 5 mm with overlaps of 0.12 mm, laser power of 195 W, laser speed of 1083 mm/s and hatch distance of 0.09 mm were set. The printing speed would be higher in this section. Upskin is indicated as the two topmost layers of the printed part to provide a suitable surface finishing. The laser power of 135 W and laser speed of 800 mm/s were selected for these layers. Contour data set the parameters for the circumference of the sample and inner side features. Laser power of 110 W and laser speed of 800 mm/s were set as the contour exposure parameters. In each layer, the laser scans the powder surface, in which, the scanning direction alters by 32°.

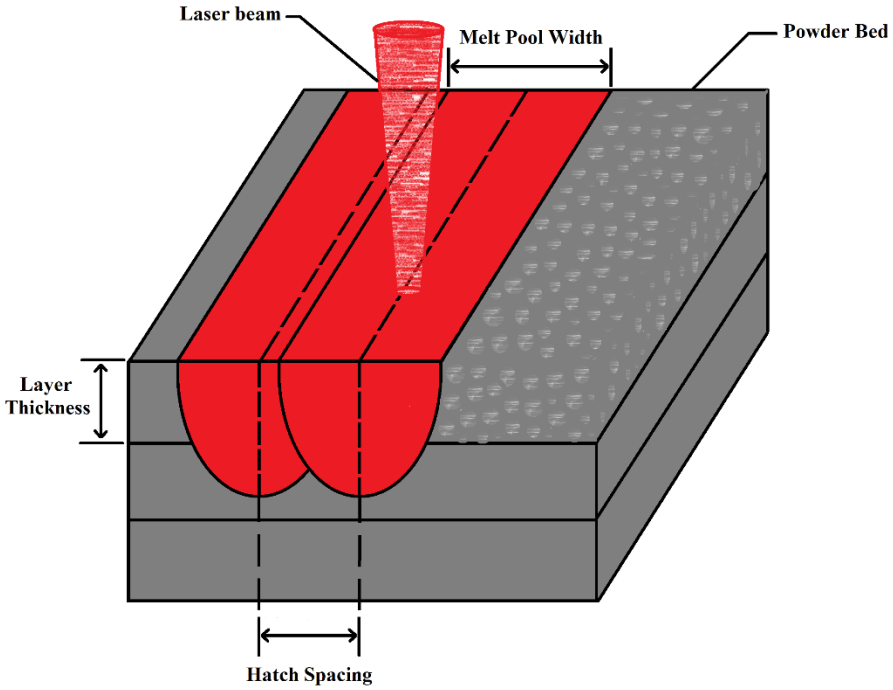

Figure 16. An illustration of the interaction between the laser beam and the powder bed.

5.3. Characterization

The powder particles size distribution was measured by Malvern Panalytical Mastersizer 2000 laser diffraction testing instrument (Figure 17). In this measuring method, the dispersed powder particles are hit by a laser beam. As the result, scattering of the laser light occurs at a large angle range. The intensity of scattered light is measured by detectors at certain positions. The particles size distribution is generated by applying a mathematical model. In this study, the stainless steel particles were dispersed in water and APB particles were dispersed in ethanol. The mixtures were agitated to prevent sedimentation. The particle size distributions are reported as the average of five carried out measurements.

Figure 17. The Malvern Panalytical Mastersizer 2000 laser diffraction testing equipment used for measuring the powder particles size distribution.

Archimedes method was applied to measure the density of compact materials, i.e. the sintered stainless steel without space-holder and 3D-printed samples with no features. Figure 18a demonstrates the apparatus of weighing machine (Sartorius CPA224S) used for density measurement. This weighing machine has an accuracy of 0.1 mg. The Vickers microhardness measurement machine (Innovatest Nexus 4303) is demonstrated in Figure 18b. In this measurement, a load of 100 g was applied for 10 s using a pyramidal diamond indenter. The hardness value is measured by microscope for the two diagonals of the indention left on the surface. The reported hardness for each indentation is the average of these two values.

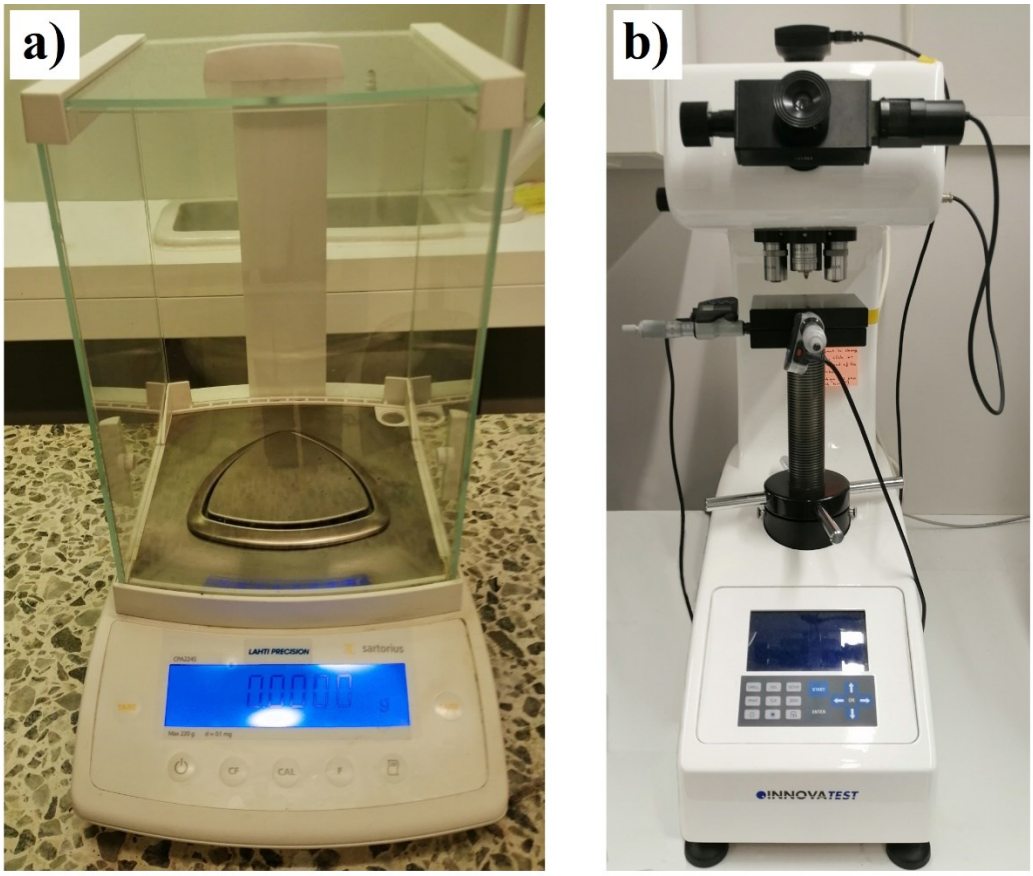

Figure 18. The apparatus of a) Sartorius CPA224S weighing machine used for density measurement and b) the apparatus of Innovatest Nexus 4303 device used for microhardness measurement.

To calculate the density, the weights of the samples were measured in air. It was followed by measuring the weight in water. The following equation was used to calculate the density of the compact materials:

$$\rho = \frac{W(a)\,.\,\rho(fl)}{G} \qquad \text{Equation 1}$$

In this equation, ρ is the density of the sample, W(a) is the weight of the sample in air, ρ(fl) is the fluid density, and G = W(a) – W(fl), considered as the buoyancy of the immersed sample, where the W(fl) indicates the weight of the sample in the fluid. In

this equation, the effect of rising level of water due to the insertion of samples is disregarded.

In order to study the fabricated materials, it is required to carry out a sample preparation to remove scratches and obtain a flat surface. Therefore, the samples were grinded using SiC papers of 240, 400 and 1200 grit by Struers LaboPol-21 grinding machine (Figure 19a). The sample were cut to analyze the cross-section of the samples. The cutting process was performed using IsoMet 4000 cutting machine by a cubic boron nitride (CBN, Buehler IsoCut®) blade with a blade speed of 2800 rpm. Figure 19b shows a general view of the cutting machine. After this step, the prepared samples were investigated by optical microscope (Leica DMRX) to provide visual information of both cross-section and external surfaces of the samples (Figure 19c).

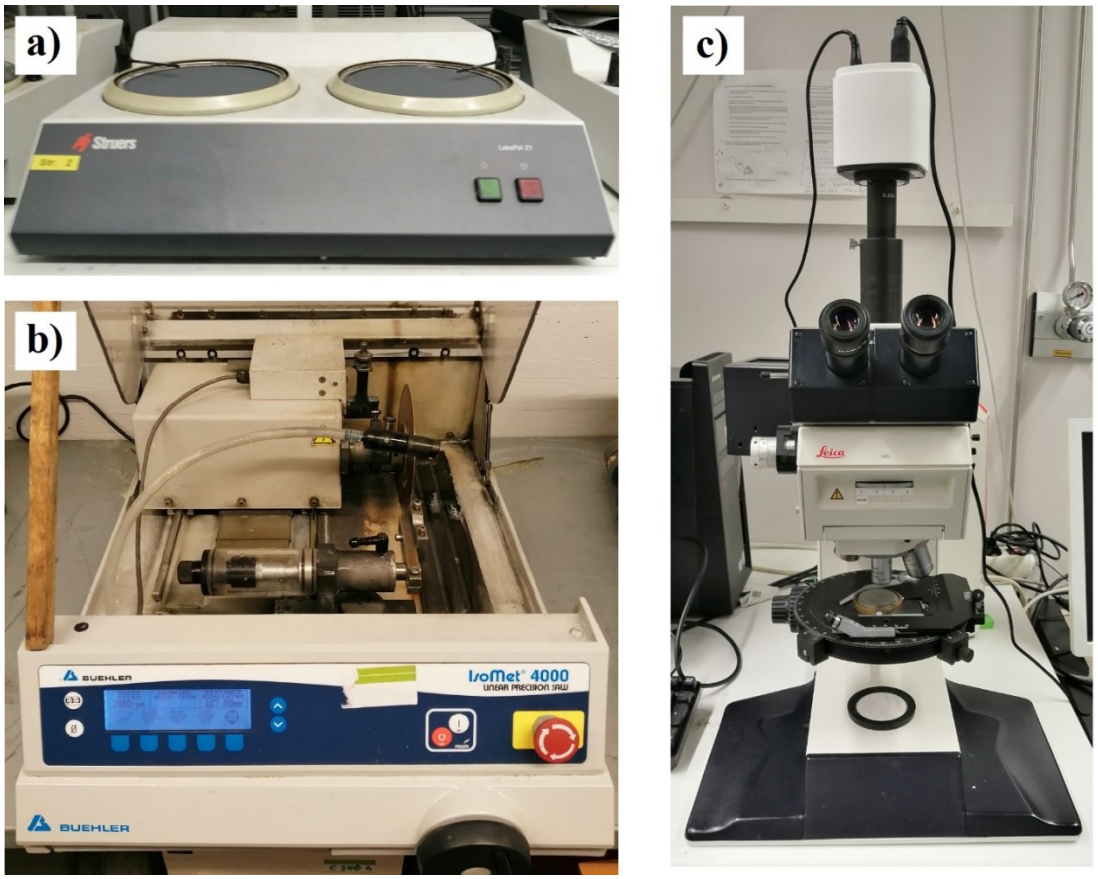

Figure 19. a) The grinding machine, b) The IsoMet 4000 cutting machine used for cutting in order to prepare cross section of specimens and c) a view Leica DMRX optical microscope.

The microstructures of the samples fabricated by both space-holder method and 3D-printing were prepared for analysis by a chemical etching process. The grinded samples were polished using 5 µm, 1 µm, 300 nm, and 50 nm alumina particles as the abrasive. Figure 20a shows the used Pheonix 4000 polishing machine. Between each of these steps, the samples were sonicated using an ultrasonic bath (FinnSonic M3, Figure 20b) in ethanol for 5 minutes in order to remove the excess particles and contamination of the surface. Separate polishing cloth was dedicated to each of these steps to avoid the presence of already existing large particles.

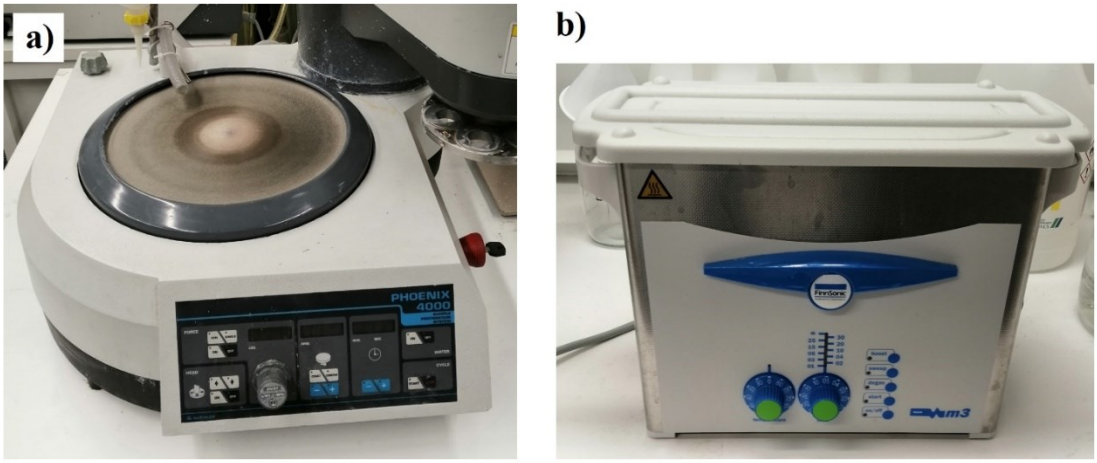

Figure 20. a) Pheonix 4000 polishing machine and b) the FinnSonic M3 ultrasonic bath.

To perform the etching process, a pre-made solution containing 1 mL of HNO_3, 45 mL of HCl, and 1 g of $CuCl_2.2H_2O$ was used. The polished surfaces were placed in the etchant solution for 16 seconds in order to reveal microstructural features. After etching, the samples were rinsed with water, ethanol and finally dried. The surfaces were then analyzed using optical microscope. Scanning electron microscopy (SEM, Hitachi-S4700) was used to study the revealed microstructure, as well as the morphology of the pores. Figure 21 shows a general view of the scanning electron microscope.

Figure 21. A general view of the scanning electron microscope (Hitachi-S4700)

6. Results

6.1. Powder

Table 6 presents the powder size distributions of the powders used for preparation of the samples, including ABP and stainless steel 316L powders used in space-holder method and powder bed fusion technique. The obtained particle sizes from laser diffraction measurement are presented as the characteristic d_{10}-d_{50}-d_{90} values.

Table 6. Numerical information on the powder particles size distribution.

Material	**Nominal Raw Material Size (µm)**	**Particle Size Distribution (µm)**		
		d_{10}	**d_{50}**	**d_{90}**
ABP	32-63	22.4	50.8	96.2
	63-90	45.4	69	102
	90-150	88.2	127	183
	150-300	147	230	358
316L (Space-holder method)	d_{80} = 22 µm	5.72	13.2	27.1
316L (PBF)	d_{50} = 37 µm	23.4	35.6	54

Figure 22 shows the graphical result of the particles size distribution of the powders. It is observed that the mean particles size of the PBF powder is almost three times that of the space-holder method. Unlike the narrowly distributed stainless steel particles used in PBF method, the smaller powder particles in space-holder method has a broad curve indicating the presence of undesired particles. The ABP powders were initially sieved to the sizes of 32-63 µm, 63-90 µm, 90-150 µm, 150-300 µm. The graphical results of the particles size distribution, however, show that there are particles out of

these margins. The smaller particle can be removed by further sieving process. The larger particles indicate the fact that ABP particles tend to agglomerate in air.

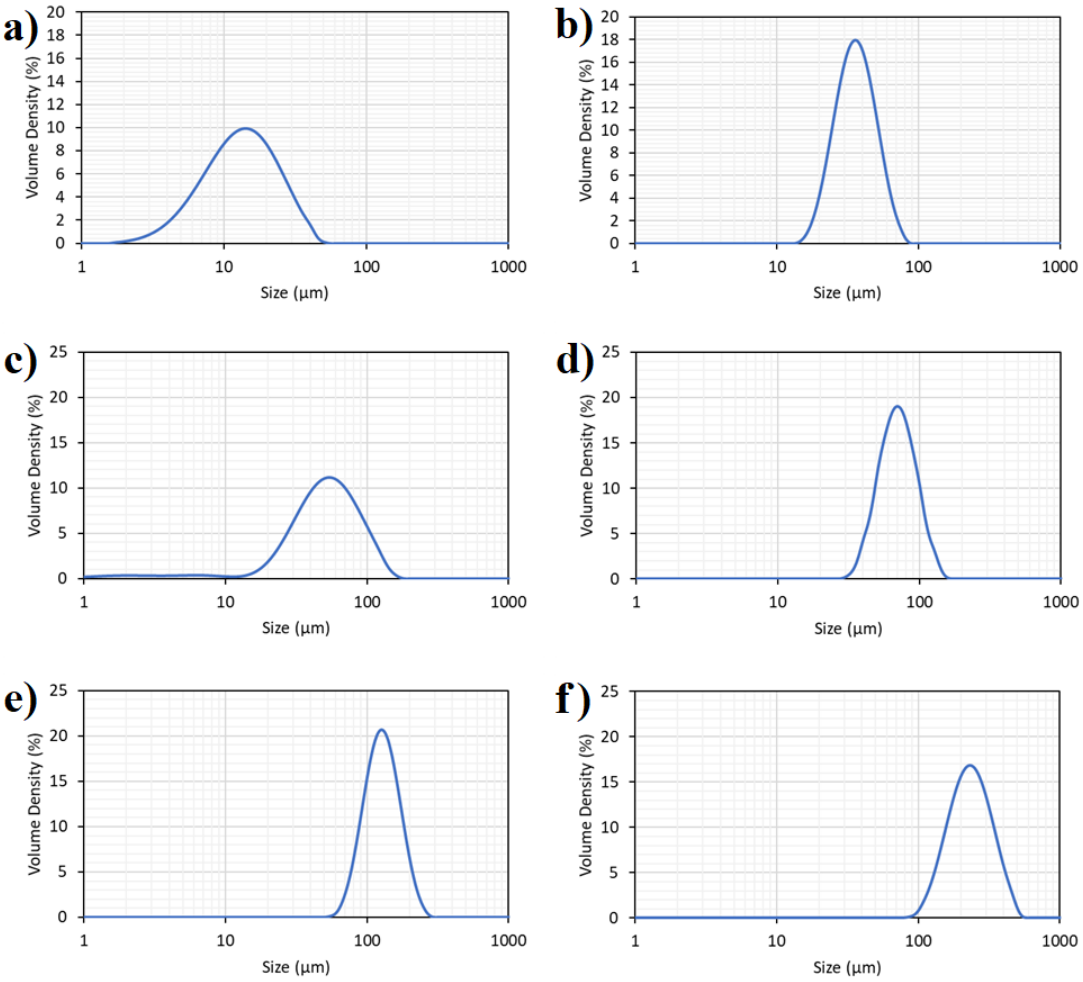

Figure 22. Powder size distribution curves of a) stainless steel 316L (space-holder method), b) stainless steel 316L (PBF method), and ABP particles with the sizes of c) 32-63 µm, d) 63-90 µm, e) 90-150 µm, and f) 150-300 µm.

The powder particles of stainless steel 316L for both space-holder method and PBF were also imaged by SEM (Figure 23). The sphericity of particles is confirmed in both powders. On the contrary, the sizes are clearly dissimilar. The PBF powders are noticeably larger and have a more uniform and comparable size.

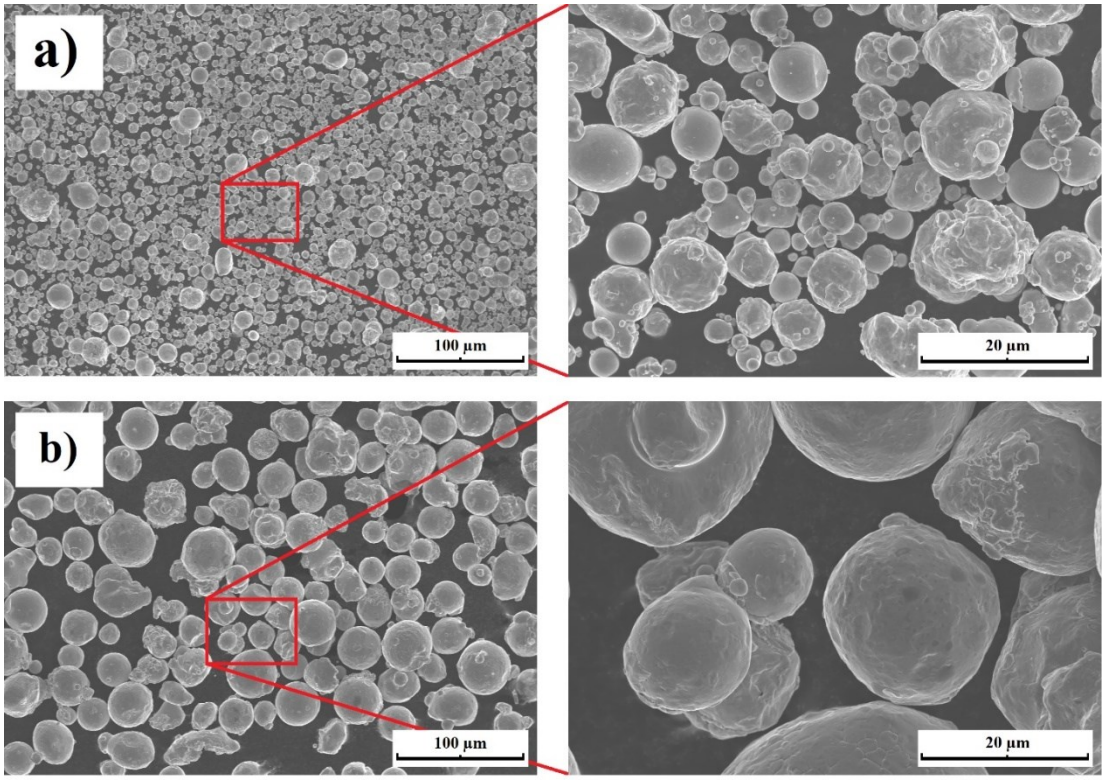

Figure 23. SEM images of stainless steel powder used in a) space-holder method, and b) PBF.

6.2. Density and hardness

Table 7 presents the densities of the compact samples prepared by sintering and powder bed fusion techniques. The densities are calculated using Equation 1. Relative densities are provided considering a density of 7.99 g/cm^3 for a fully dense sample. The microscopic images have been also used to calculate the porosities by image analysis. The results from density measurement suggest that the sintering process lead to a lower density.

Table 7. The density and Vickers microhardness of compact samples.

Method	Density (g/cm^3)	Relative Density (%)	Calculated Porosity by image analysis (%)
Sintering	6.89	87.02	12.28
Powder Bed Fusion	7.87	98.4	0.76

Figure 24 shows the surfaces of the compact materials. The sintered stainless steel has noticeable number of pores. The pores, mostly, have a size of less than 10 µm. On the other hand, the 3D-printed sample has smooth surface with few defects.

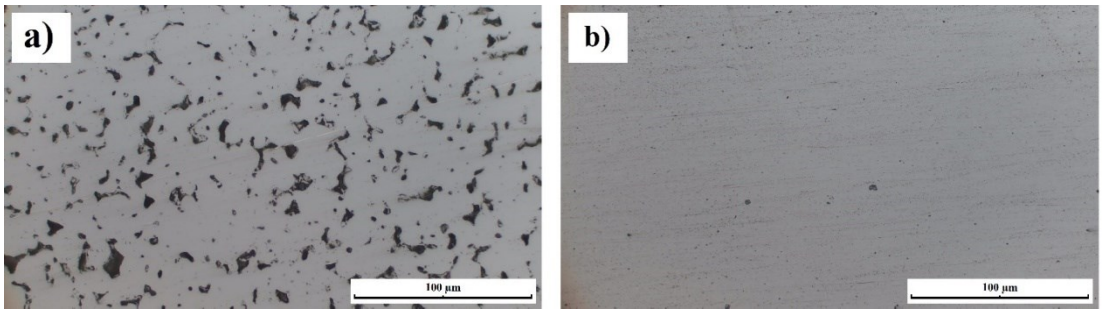

Figure 24. The optical images of compact stainless steel 316L samples fabricated by a) sintering and b) PBF.

The obtained Vickers microhardness value of the compact stainless steel 316L samples are graphically presented in Figure 25. The mean values and respective standard deviations are calculated by performing seven indentations. It is observed that the hardness of 3D-printed sample is noticeably higher than that of space-holder method.

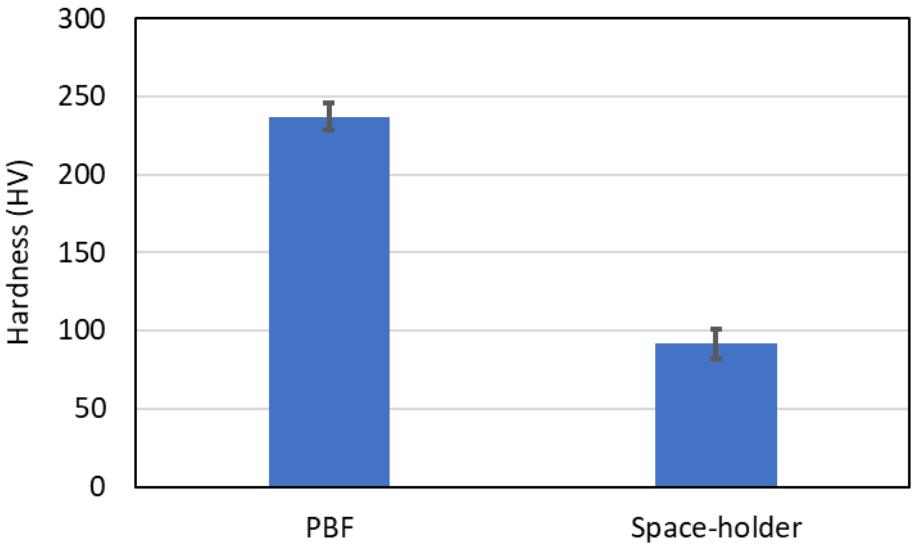

Figure 25. The Vickers microhardness of the compact 316L materials prepared by different methods.

6.3. Pore formation

6.3.1. Space-holder method

Figure 26 shows the cross-sectional images of the samples prepared by space holder method, containing nominal volume fractions of 50, 60, 70, and 80%. The used space-holder powder had a nominal size of 150-300 µm. The successful formation of pores is clearly visible. The walls thicknesses decrease by the addition of space holder volume fraction. For volume fraction of 50%, an uneven distribution of pores is observed. The pores in sample with 80% of porosity are deformed after removal of the space-holder particles, due to the very thin cell walls.

The cross-sectional images of the samples with different volume fraction of space-holder were analyzed to calculate the actual porosities. Figure 27 shows the calculated porosities for each sample. It is observed that the porosities are lower comparing to the initial volume fraction of space-holder powders.

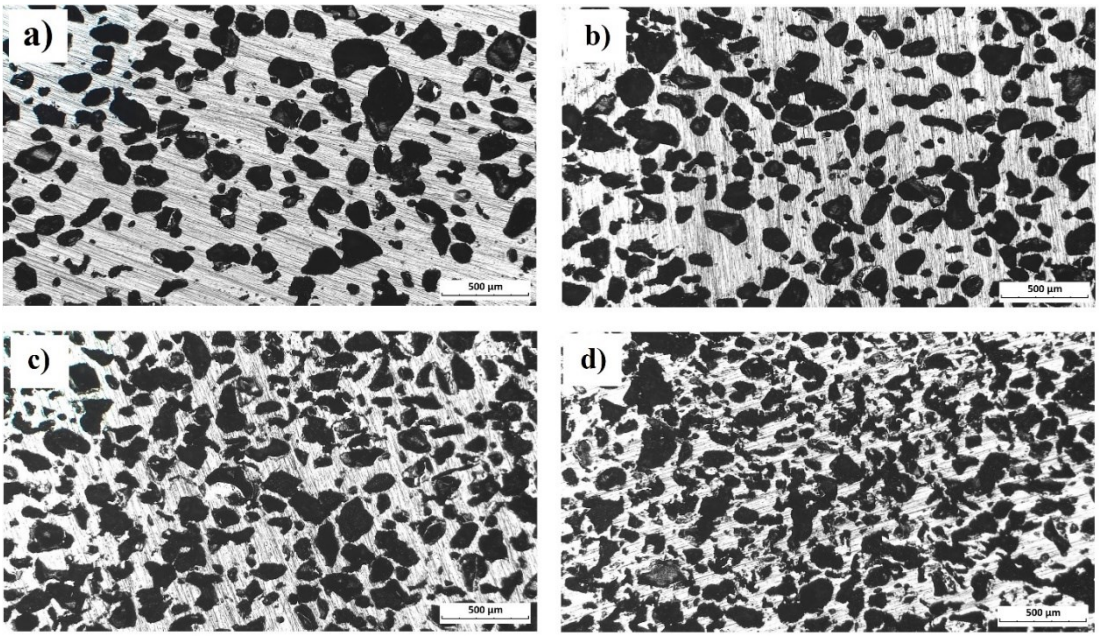

Figure 26. Cross-sectional images of samples with various volume fractions of space-holder. The space-holder powder size is 150-300 µm.

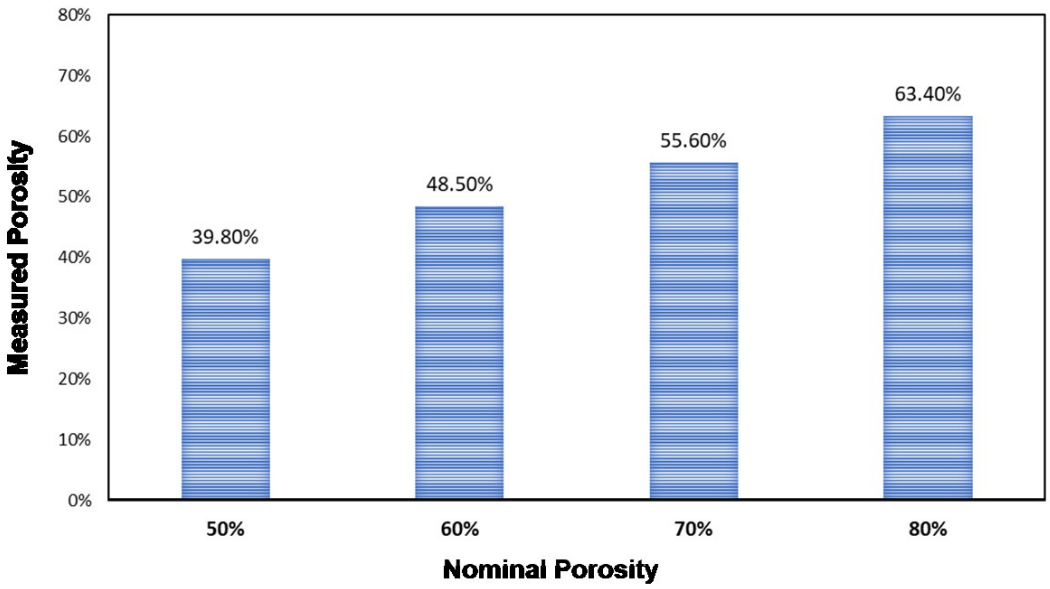

Figure 27. A comparison between the nominal porosity and the calculated porosity of samples.

Figure 28 demonstrates the cross-sectional images of the samples with different space-holder particles sizes. In all cases, the volume fraction of the space-holder is kept

constant and equal to 70%. The wall thickness sizes have decreased by reducing the space-holder particle size. In Figure 28, an accumulation of pores has generated larger pores in several locations.

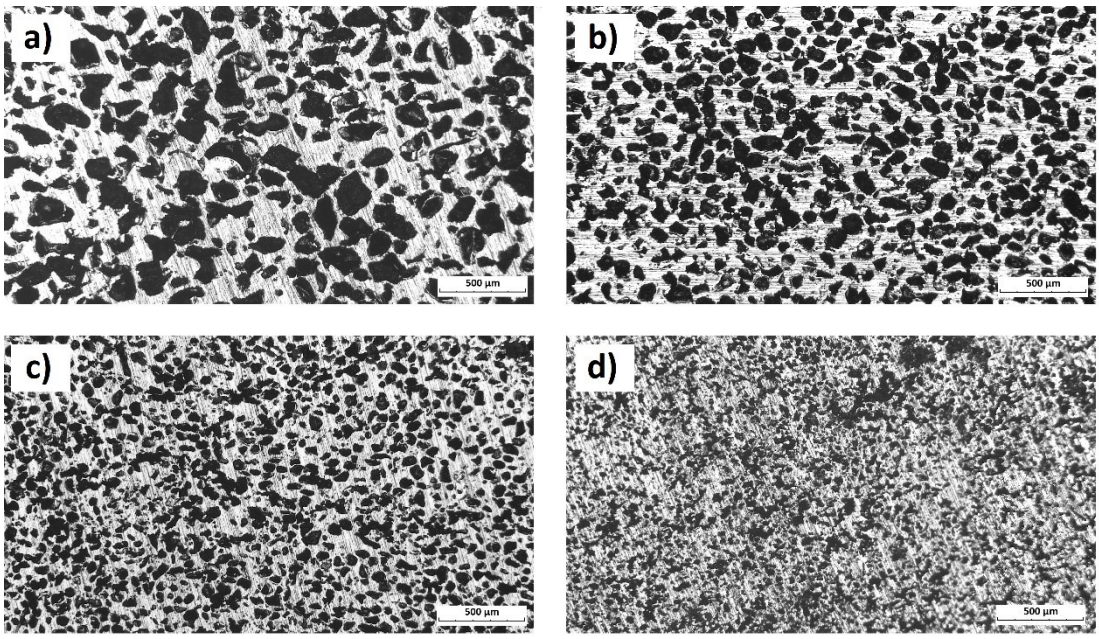

Figure 28. Cross-sectional images of samples with 70% volume fractions of space-holder. The space-holder nominal powder sizes are a) 150-300 µm, b) 90-150 µm, c) 63-90 µm, and d) 32-63 µm.

The porosities were also calculated for the samples with different space-holder particle sizes using the cross-sectional images. The calculated porosities are shown in Figure 29. The results demonstrate a solidarity of porosities, indicating that the shrinkage has happened equally in all cases.

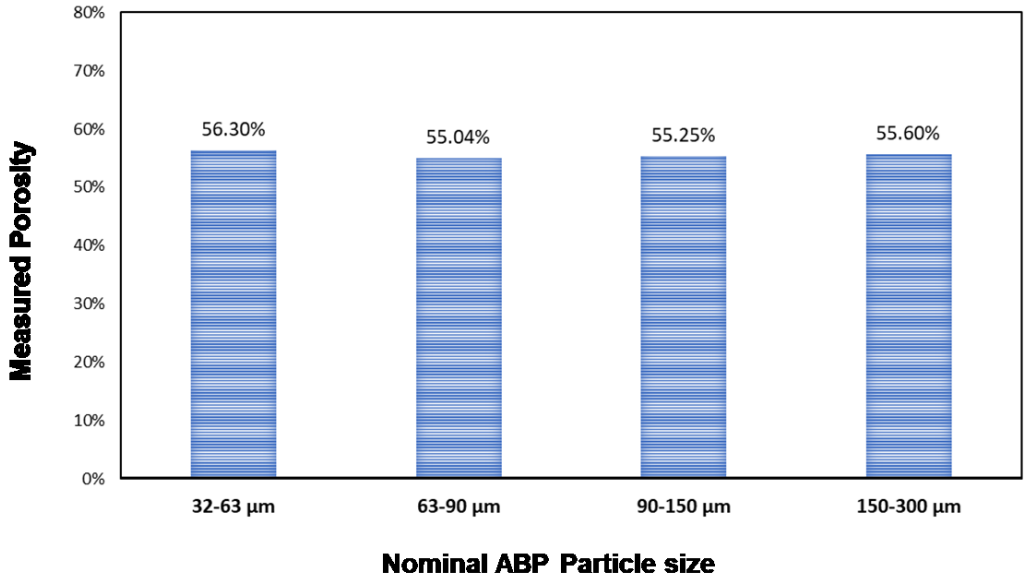

Figure 29. The calculated porosities of the samples with nominal porosity of 70% and various space-holder (ABP) particle sizes.

The fabrication of a porous structure with a gradient in the pore sizes has been carried out using the space-holder sizes of 63-90 µm, 90-150 µm, and 150-300µm. Figure 30 demonstrates that the sample has been successfully fabricated. The boundary line between the 63-90 µm and 90-150 µm is not as distinguishable as that of 90-150 µm and 150-30 µm. Accumulated pores with notably larger pore sizes are observed in the areas with both 63-90 µm and 90-150 µm pore sizes. These structures can improve the efficiency of the filters by improving the fluid flux and amending the retention rate.

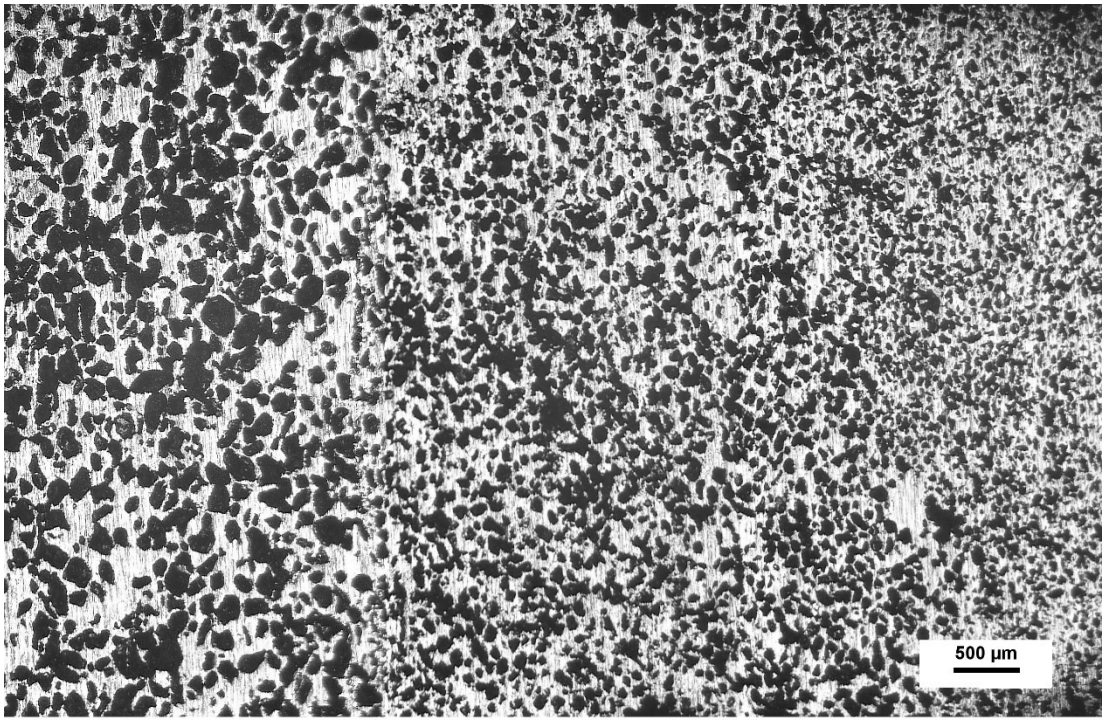

Figure 30. Cross-sectional image of a sample with 70% volume fractions of space-holder. From left to right, the gradient of space-holder powder nominal sizes of 150-300 µm, 90-150 µm, 63-90 µm.

Figure 31 shows the morphology of the formed pores in a sample with space-holder particle sizes of 150-300 µm. It can be inferred that the pores are formed by several space-holder particles and resulted the formation of interconnecting pores. The size range of these interconnections is considerably less than the space-holders. The surface of the pores is smooth and indicate an acceptable level of sintering.

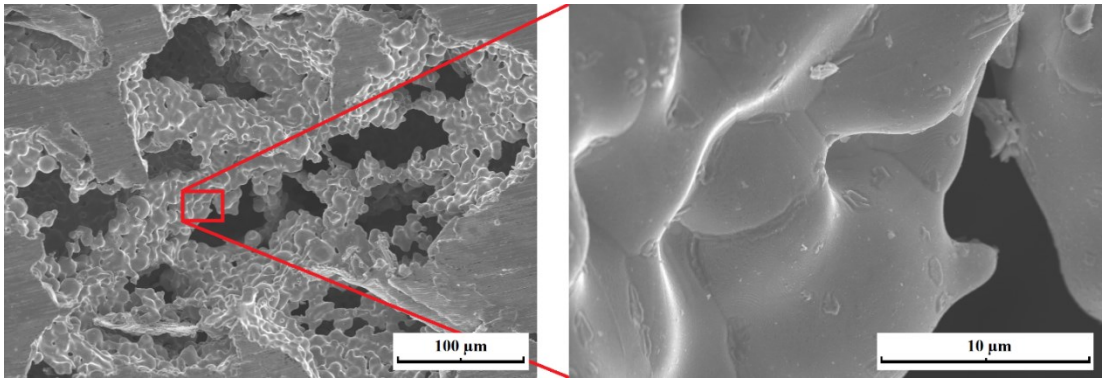

Figure 31. SEM images of pores formed from a nominal space-holder size of 150-300 µm.

Figure 32 presents the etched surface of the free sintered stainless steel sample. It can be seen that the grains are in the scale of several micrometers. Also, the presence of a twinned grain can be noted. The grain size would directly affect the final mechanical properties of the fabricated materials. Presence of a twinned grain can be noted.

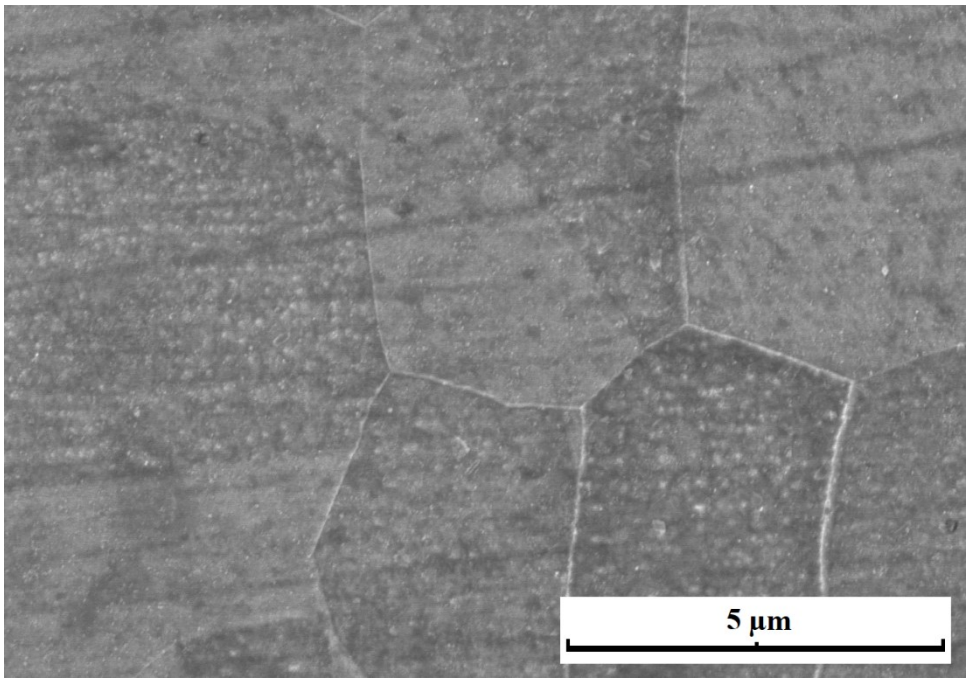

Figure 32. SEM image of the etched free sintered stainless steel.

6.3.2. Powder bed fusion (PBF)

Figure 33 shows the top and cross-sectional views of the cylindrical channels prepared by PBF method. In all cases, the diameters are approximately 50 µm smaller than designed. The channels tend to have less repeatable shape as the diameter decreases. Although a minimum channel size of 150 µm, the removal of residual powder from the channels is problematic. As a result, the minimum channel sizes were close-ended before cross-sectioning. In contrast, the wall thicknesses expanded comparing to the designed 100, 200, 300, 400, and 500 µm sizes. This increase also has an extent of ~50

µm. The microscopic images show that a minimum wall thickness of 150 µm is achievable for this geometry.

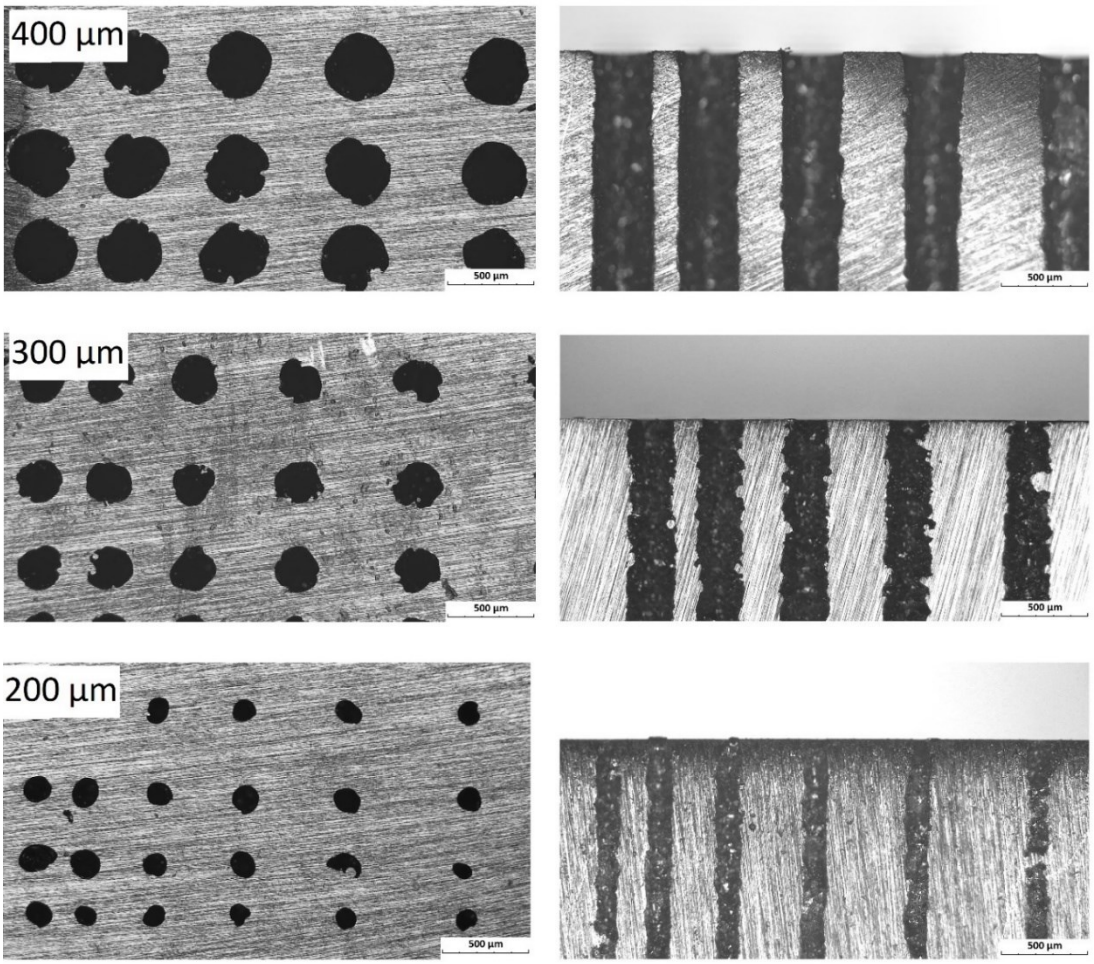

Figure 33. Cross-sectional images of the cylindrical channels prepared by the powder bed fusion method.

The cross-sectional SEM images of the conical and pyramidal channels are given in Figure 34. The gradual transform from a wide to narrow end can be noted. The shrinkage of the channel is also visible in these cases. The designed 500 µm wide end of the channel yields in 450 µm, and the narrow end of 300 µm result a 250 µm diameter. The latter seems to be less of a concern in the case of pyramidal channel, since the shrinkage is not as severe. The surface morphologies seem quite similar in both cases. Several particles are partially fused to the surface. These particles could not be removed by sonicating and pressurized air flow.

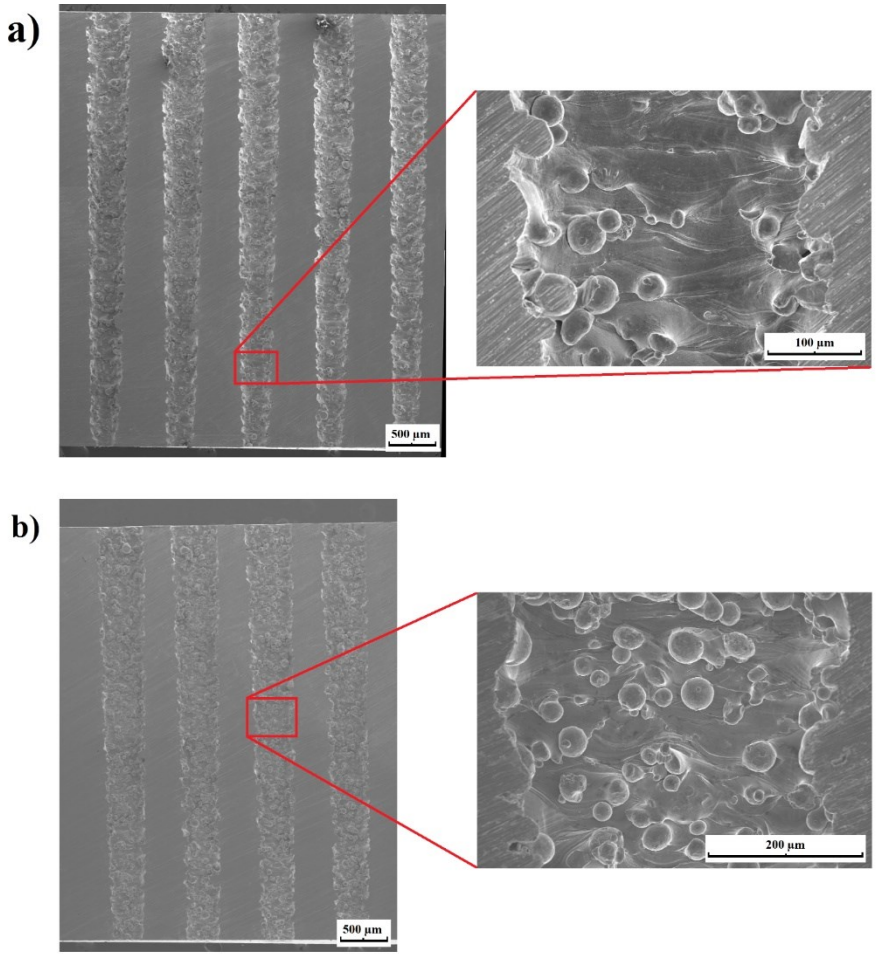

Figure 34. Cross-sectional SEM image of a) conical and b) pyramidal channels prepared by powder bed fusion (PBF) method.

Figure 35 shows the representative optical images of the etched 3D-printed stainless steel. A layered microstructure can be noted from this figure, addressing the generated melt pools during the additive manufacturing process. Large columnar grains, growing in the direction of thermal gradient, are also observed within the melt pools.

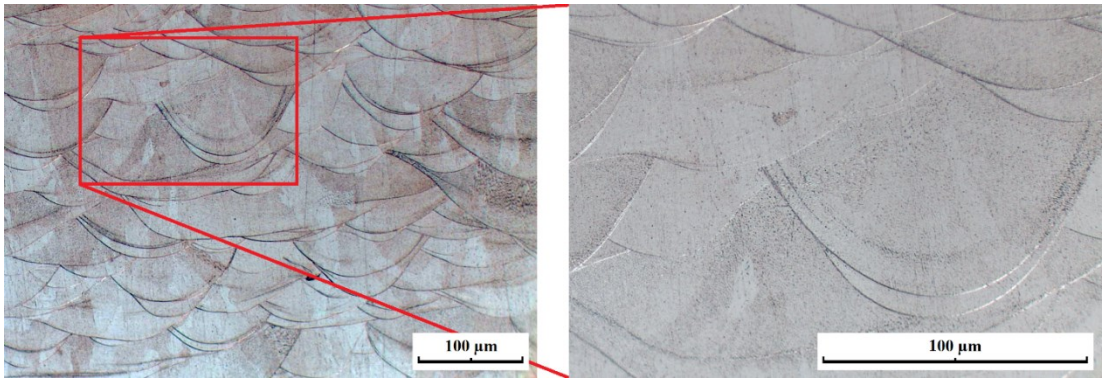

Figure 35. Representative optical images of the 316L sample prepared by PBF.

Figure 36 presents SEM images of the melt pools. The higher magnification of these images clearly shows the cellular structure, typically observed in laser processed materials. The cells have polygonal shapes elongated in different directions. Various cell sizes are noted, however, the they do not exceed 2 µm.

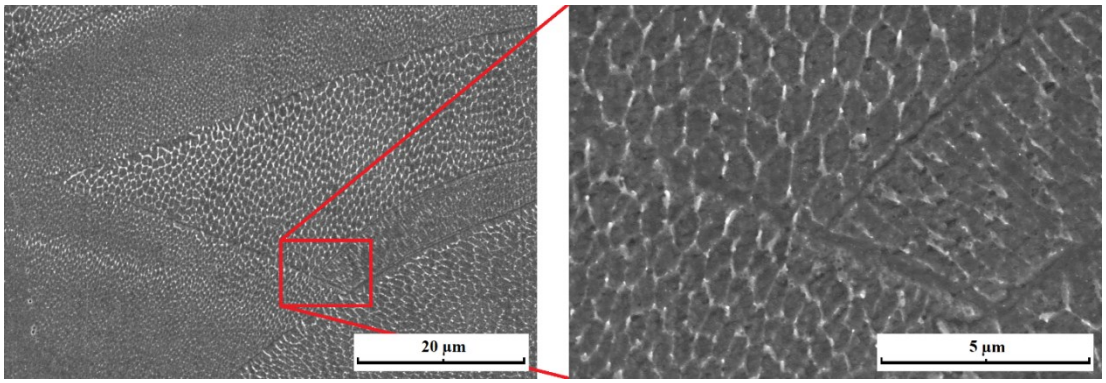

Figure 36. SEM images of lateral side of PBF samples, showing the typical cellular structures observed in 316L.

7. Discussion

7.1. Space-holder method

The usage of space-holder was investigated as the pore forming agent in sintered materials. In this method, the fine stainless steel powders coat space-holder particles, which are later removed and subsequently provide the desired pores. The ratio of metal to space-holder is very important in formation of inter-connected pores. It can be inferred that the mechanical properties are also significantly influence by this ration due to its influence on the cell wall thickness.

The final porosities were noted to be less than the volume fraction of initially inserted space-holder particles due to shrinkage. The shrinkage found to be relatively less comparing to previous works with larger initial stainless steel powder size [48]. This is consistent with previous study by Nishiyabu et al. [56], showing the minimum powder particle size for the matrix and maximum space-holder particle size yield in the most favorable result. Also, usage of ABP instead of PMMA as space-holder material has considerably reduced the required time and temperature for space-holder removal in this thesis.

The microscopic images reveal the presence of few larger pores than the used space-holder particles. The larger pores indicate the fact that ABP particles tend to agglomerate, which has been previously reported [86]. This is especially observed in particles with minimum size ranges, i.e. 32- 63 μm.

Scanning electron microscopy was also utilized to assess the possibility of microstructure analysis. The microstructure was revealed by proper etching process. Considering the dependency of grain size on process temperature and duration [3], the comparably large grains size of sintered samples is because of the long duration of sintering. The grains have a size of several micrometers, appearing to have similar size to that of the initial fine powder.

The results from density measurement suggest that the sintering process lead to a lower density, comparing to the 3D-printed samples. It is also observed that the hardness of the 3D-printed sample is noticeably higher than that of space-holder method. This is

this can be referred to as the result of lower porosity of the sintered samples. The measured hardness agrees well with that observed by Kurgan [87]. It has been suggested that 50-100 ℃ increase of the sintering temperature can further improve the mechanical properties.

The pores in the sample with 80% of porosity are deformed after removal of the space-holder particles. It can be deduced that the shrinkage is due to the thin cell walls and can be considered as a limiting factor for fabrication of highly porous structures.

The fabrication of a porous structure with a gradient in pores sizes has been successfully accomplished. It is suggested [88] that pore gradient structures can improve the efficiency of the filters by improving the fluid flux and amending the retention rate.

7.2. Powder bed fusion

The minimum wall thickness was limited by the laser beam size. The microscopic images showed that the minimum channel size of 300 µm is achievable. In the case of smaller channel sizes, powder removal was not feasible. A minimum wall thickness of 150 µm was successfully printed. This size is limited by the 100 µm size of laser beam, which leads to a ~150 µm wide melt pools. The sizes of melt pools are confirmed by lateral microscopic images.

In an attempt [89] on Inconel 625 using selective laser melting method, it was reported that the fabrication of channels with diameters less than 600 µm was not successful. Also, the minimum achievable hole feature had a diameter of 300 µm and only a minimum depth (i.e. close-ended). In this study, 3D-printing of channels with gradient in size facilitates the removal the residual powder from the wide end of the channels. In this case, a minimum printable channel diameter of 250 µm has been accomplished.

The grain boundaries and melt pool lines were revealed by etching the 3D-printed samples. Large and elongated grains are observed in the structure. Each of these grains include numerous columnar cells in the sub-micrometer scale. The growth of these

cells is suggested [90] to be in opposite direction of highest thermal gradient. Also, the size of these cells would grow in the areas with lower cooling rates.

The cellular structures of the melt pools are ascribed to the high cooling rate leading to a condition of non-equilibrium solidification [91]. This solidification often possesses a strong directionality, in which the solidification begins on melt pool boundaries and directs toward the center of melt pools [90]. The resulting directionality and grain morphology are controlled by temperature gradient and growth rate of solid front.

The measured hardness of 3D-printed sample is in agreement with that observed for identical laser energy and resulting porosity by Cherry *et al.* [92]. It is suggested that the hardness would decrease by increasing the porosity. The minimum density was recorded for the laser power of 104 J/mm^3.

The recorded density of 98.4% differs from that previously 99.5% value reported for identical printing system with an exception of lower hatch spacing [90]. This result is compatible with those noted in a research by Sun et al. [93], suggesting a maximized density by decreasing the hatch spacing from nominal size of 0.12 mm. Pores in the scale of several micrometers are observed, corresponding to entrapped gas bubbles.

8. Conclusion

This thesis has reviewed various sintering methods and additive manufacturing techniques and assessed their applicability to fabricate porous filter media. The studied porous media consisted of metallic, ceramic and polymeric materials. Furthermore, the porous stainless steel 316L have been developed using both space-holder sintering method and powder bed fusion technique.

The space-holder method consists of sacrificial particles that are mixed with the stainless steel powder and compacted. These particles are removed to form pores inside the green compact, which is then sintered to form a solid porous medium. The size and volume fraction of space-holder particles defines the final structure. The volume fraction of space-holder particles determines the final porosity of the sintered material, however, a shrinkage has been recorded after characterization of the porosity. The porosity has a similar range of shrinkage for all ranges of pore sizes with constant volume fraction. This method provided the possibility to simply fabricate structures with a gradient pore sizes, promoting the filtering capability of porous filter medium.

Stainless steel parts containing channels with various diameters, cross-sections and wall thicknesses have been designed, fabricated, and characterized using laser powder bed fusion technique. The channels with square-shaped cross sections tend to have round corners, especially in smaller scales. Channels smaller than 400 µm have a desirable shrinkage of ca. 50 µm. As the result, channels with minimum diameter of 250 µm can be successfully produced from initially 300 µm designed channels. The smallest printable feature has a diameter of 200 µm, however, the depth would be still limited due to the difficulty of residual powder removal. The successfulness of designed channels with a gradient in size can be a promising approach for the future studies.

The samples fabricated by powder bed fusion technique possess a superior hardness and density comparing to those of a sintered sample. The lower hardness of sintered sample is addressed to the long holding time at high temperatures. Their density can be improved by optimizing the amount of binder.

The pores formed by the space-holder method have had a smooth surface. On the contrary, the channels side walls of samples produced by PBF technique illustrate the presence of numerous partially fused powder particles on the channel walls.

The developed space-holder method in this thesis only optimizes the porosity and pore sizes by controlling the initial size and volume fraction of sacrificial particles. However, the density of compact parts, hardness, porosity and pore shapes might be improved by adjusting the sintering parameters. These properties could be enhanced by optimizing the sintering temperature, stainless steel powder size distribution or the compacting pressure.

9. References

[1] Olevsky EA. Theory of sintering: from discrete to continuum. Materials Science and Engineering: R: Reports. 1998 Jun 30;23(2):41-100.

[2] German RM. Sintering theory and practice. Solar-Terrestrial Physics. 1996 Jan:568.

[3] Kang SJ. Sintering: densification, grain growth and microstructure. Elsevier; 2004 Nov 27.

[4] German RM. Liquid phase sintering. Springer Science & Business Media; 2013 Dec 14.

[5] German RM, Suri P, Park SJ. liquid phase sintering. Journal of materials science. 2009 Jan 1;44(1):1-39.

[6] Markaki AE, Gergely V, Cockburn A, Clyne TW. Production of a highly porous material by liquid phase sintering of short ferritic stainless steel fibres and a preliminary study of its mechanical behaviour. Composites science and technology. 2003 Dec 1;63(16):2345-51.

[7] Li W, Olevsky EA, McKittrick J, Maximenko AL, German RM. Densification mechanisms of spark plasma sintering: multi-step pressure dilatometry. Journal of Materials Science. 2012 Oct 1;47(20):7036-46.

[8] Olevsky EA, Kandukuri S, Froyen L. Consolidation enhancement in spark-plasma sintering: Impact of high heating rates. Journal of Applied Physics. 2007 Dec 1;102(11):114913.

[9] Orru R, Licheri R, Locci AM, Cincotti A, Cao G. Consolidation/synthesis of materials by electric current activated/assisted sintering. Materials Science and Engineering: R: Reports. 2009 Feb 12;63(4-6):127-287.

[10] Keller C, Tabalaiev K, Marnier G, Noudem J, Sauvage X, Hug E. Influence of spark plasma sintering conditions on the sintering and functional properties of an ultra-fine grained 316L stainless steel obtained from ball-milled powder. Materials Science and Engineering: A. 2016 May 17;665:125-34.

[11] Cavaliere P, editor. Spark plasma sintering of materials: advances in processing and applications. Springer; 2019 Feb 18.

[12] Sairam K, Sonber JK, Murthy TC, Sahu AK, Bedse RD, Chakravartty JK. Pressureless sintering of chromium diboride using spark plasma sintering facility. International Journal of Refractory Metals and Hard Materials. 2016 Aug 1;58:165-71.

[13] Yamanoglu R, Gulsoy N, Olevsky EA, Gulsoy HO. Production of porous Ti5Al2. 5Fe alloy via pressureless spark plasma sintering. Journal of Alloys and Compounds. 2016 Sep 25;680:654-8.

[14] Łazińska M, Durejko T, Lipiński S, Polkowski W, Czujko T, Varin RA. Porous graded FeAl intermetallic foams fabricated by sintering process using NaCl space holders. Materials Science and Engineering: A. 2015 Jun 11;636:407-14.

[15] Kubota M. Properties of nano-structured pure Al produced by mechanical grinding and spark plasma sintering. Journal of Alloys and Compounds. 2007 May 31;434:294-7.

[16] Fais A. Processing characteristics and parameters in capacitor discharge sintering. Journal of materials processing technology. 2010 Nov 19;210(15):2223-30.

[17] Fais A, inventor; EPOS SRL, assignee. Sintering process and corresponding sintering system. United States patent US 9,227,244. 2016 Jan 5.

[18] German R. Sintering: from empirical observations to scientific principles. Butterworth-Heinemann; 2014 Feb 7.

[19] Hu C, Li F, Qu D, Wang Q, Xie R, Zhang H, Peng S, Bao Y, Zhou Y. Developments in hot pressing (HP) and hot isostatic pressing (HIP) of ceramic matrix

composites. In Advances in Ceramic Matrix Composites 2014 Jan 1 (pp. 177-202). Woodhead Publishing.

[20] Kumar LJ, Pandey PM, Wimpenny DI, editors. 3D printing and additive manufacturing technologies. Singapore: Springer; 2019.

[21] Kretzschmar N, Chekurov S, Salmi M, Tuomi J. Evaluating the readiness level of additively manufactured digital spare parts: an industrial perspective. Applied Sciences. 2018 Oct;8(10):1837.

[22] Tuomi J, Paloheimo K, Björkstrand R, Salmi M, Paloheimo M, Mäkitie AA. Medical applications of rapid prototyping-from applications to classification. In4th International Conference on Advanced Research in Virtual and Rapid Prototyping 2010 (pp. 701-704). TAYLOR & FRANCIS LTD.

[23] Vaezi M, Seitz H, Yang S. A review on 3D micro-additive manufacturing technologies. The International Journal of Advanced Manufacturing Technology. 2013 Jul 1;67(5-8):1721-54.

[24] Linxi Z, Quanzhan Y, Guirong Z, Fangxin Z, Gang S, Bo Y. Additive manufacturing technologies of porous metal implants. China Foundry. 2014 Jul 1;11(4):322-31.

[25] Yang L, Hsu K, Baughman B, Godfrey D, Medina F, Menon M, Wiener S. Additive manufacturing of metals: the technology, materials, design and production. Schwitzerland: Springer; 2017 May 11.

[26] Wang D, Yang Y, Liu R, Xiao D, Sun J. Study on the designing rules and processability of porous structure based on selective laser melting (SLM). Journal of Materials Processing Technology. 2013 Oct 1;213(10):1734-42.

[27] Manfredi D, Calignano F, Krishnan M, Canali R, Ambrosio EP, Atzeni E. From powders to dense metal parts: Characterization of a commercial AlSiMg alloy processed through direct metal laser sintering. Materials. 2013 Mar;6(3):856-69.

[28] Aboulkhair NT, Simonelli M, Parry L, Ashcroft I, Tuck C, Hague R. 3D printing of Aluminium alloys: Additive Manufacturing of Aluminium alloys using selective laser melting. Progress in Materials Science. 2019 Dec 1;106:100578.

[29] Calle MA, Salmi M, Mazzariol LM, Alves M, Kujala P. Additive manufacturing of miniature marine structures for crashworthiness verification: Scaling technique and experimental tests. Marine Structures. 2020 Jul 1;72:102764.

[30] Yeong WY, Sudarmadji N, Yu HY, Chua CK, Leong KF, Venkatraman SS, Boey YC, Tan LP. Porous polycaprolactone scaffold for cardiac tissue engineering fabricated by selective laser sintering. Acta biomaterialia. 2010 Jun 1;6(6):2028-34.

[31] Comb J, Priedeman W, Turley PW. FDM® Technology process improvements. In1994 International Solid Freeform Fabrication Symposium 1994.

[32] Duty C, Ajinjeru C, Kishore V, Compton B, Hmeidat N, Chen X, Liu P, Hassen AA, Lindahl J, Kunc V. What makes a material printable? A viscoelastic model for extrusion-based 3D printing of polymers. Journal of Manufacturing Processes. 2018 Oct 1;35:526-37.

[33] Ivey M, Melenka GW, Carey JP, Ayranci C. Characterizing short-fiber-reinforced composites produced using additive manufacturing. Advanced Manufacturing: Polymer & Composites Science. 2017 Jul 3;3(3):81-91.

[34] Ahn SH, Montero M, Odell D, Roundy S, Wright PK. Anisotropic material properties of fused deposition modeling ABS. Rapid prototyping journal. 2002 Oct 1.

[35] Yap YL, Wang C, Sing SL, Dikshit V, Yeong WY, Wei J. Material jetting additive manufacturing: An experimental study using designed metrological benchmarks. Precision engineering. 2017 Oct 1;50:275-85.

[36] Dikshit V, Nagalingam AP, Yap YL, Sing SL, Yeong WY, Wei J. Investigation of quasi-static indentation response of inkjet printed sandwich structures under various indenter geometries. Materials. 2017 Mar;10(3):290.

[37] Yeong WY, Chua CK, Leong KF, Chandrasekaran M, Lee MW. Development of scaffolds for tissue engineering using a 3D inkjet. InVirtual Modelling and Rapid Manufacturing: Advanced Research in Virtual and Rapid Prototyping Proc. 2nd Int. Conf. on Advanced Research in Virtual and Rapid Prototyping, 28 Sep-1 Oct 2005, Leiria, Portugal 2005 Sep 15 (p. 115). CRC Press.

[38] Sutherland KS, Chase G. Filters and filtration handbook. Elsevier; 2011 Apr 18.

[39] Banhart J. Manufacture, characterisation and application of cellular metals and metal foams. Progress in materials science. 2001 Jan 1;46(6):559-632.

[40] Murray NG, Dunand DC. Microstructure evolution during solid-state foaming of titanium. Composites science and technology. 2003 Dec 1;63(16):2311-6.

[41] Lázaro J, Solórzano E, Rodríguez-Pérez MA. Alternative carbonates to produce aluminium foams via melt route. Procedia Materials Science. 2014 Jan 1;4:275-80.

[42] Gergely V, Curran DC, Clyne TW. The FOAMCARP process: foaming of aluminium MMCs by the chalk-aluminium reaction in precursors. Composites Science and Technology. 2003 Dec 1;63(16):2301-10.

[43] Hassani A, Habibolahzadeh A, Bafti H. Production of graded aluminum foams via powder space holder technique. Materials & Design. 2012 Sep 1;40:510-5.

[44] Mapelli C, Mombelli D, Gruttadauria A, Barella S, Castrodeza EM. Performance of stainless steel foams produced by infiltration casting techniques. Journal of Materials Processing Technology. 2013 Nov 1;213(11):1846-54.

[45] Ashby MF, Evans T, Fleck NA, Hutchinson JW, Wadley HN, Gibson LJ. Metal foams: a design guide. Elsevier; 2000 Jul 30.

[46] Lu X. Fluid Flow and Heat Transfer in Porous Media Manufactured by a Space Holder Method (Doctoral dissertation, University of Liverpool).

[47] Surace R, De Filippis LA, Niini E, Ludovico AD, Orkas J. Morphological investigation of foamed aluminum parts produced by melt gas injection. Advances in Materials Science and Engineering. 2009 Jan 1;2009.

[48] Bekoz N, Oktay E. High temperature mechanical properties of low alloy steel foams produced by powder metallurgy. Materials & Design. 2014 Jan 1;53:482-9.

[49] Peroni L, Scapin M, Fichera C, Lehmhus D, Weise J, Baumeister J, Avalle M. Investigation of the mechanical behaviour of AISI 316L stainless steel syntactic foams at different strain-rates. Composites Part B: Engineering. 2014 Nov 1;66:430-42.

[50] Bakan HI. A novel water leaching and sintering process for manufacturing highly porous stainless steel. Scripta materialia. 2006 Jul 1;55(2):203-6.

[51] Mutlu I, Oktay E. Influence of fluoride content of artificial saliva on metal release from 17- 4 PH stainless steel foam for dental implant applications. Journal of Materials Science & Technology. 2013 Jun 1;29(6):582-8.

[52] Ibrahim A, Zhang F, Otterstein E, Burkel E. Processing of porous Ti and Ti5Mn foams by spark plasma sintering. Materials & Design. 2011 Jan 1;32(1):146-53.

[53] Golabgir MH, Ebrahimi-Kahrizsangi R, Torabi O, Tajizadegan H, Jamshidi A. Fabrication and evaluation of oxidation resistance performance of open-celled Fe (Al) foam by space-holder technique. Advanced Powder Technology. 2014 May 1;25(3):960-7.

[54] Jakubowicz J, Adamek G, Dewidar M. Titanium foam made with saccharose as a space holder. Journal of Porous Materials. 2013 Oct 1;20(5):1137-41.

[55] Mutlu I, Oktay E. Production and characterisation of Cr-Si-Ni-Mo steel foams.

[56] Nishiyabu K, Matsuzaki S, Tanaka S. Fabrication of Micro Porous Metal Components by Metal Injection Molding Based Powder Space Holder Method. High Temperature Materials and Processes. 2007;26(4):257-68.

[57] Hangai Y, Ando M, Ohashi M, Amagai K, Suzuki R, Matsubara M, Yoshikawa N. Compressive properties of two-layered aluminum foams with closed-cell and open-cell structures. Materials Today Communications. 2020 May 23:101249.

[58] Somiya S. Handbook of advanced ceramics: materials, applications, processing, and properties. Academic press; 2013 Apr 11.

[59] Daoush W, Moustafa S, Kayetbay S. Processing of metallic filters by powder metallurgy technique. Powder Metallurgy Progress. 2006;6(4):164-9.

[60] Da Silva Biron D, Dos Santos V, Zeni M. Ceramic membranes applied in separation processes. Springer; 2017 May 18.

[61] Gitis V, Rothenberg G. Ceramic membranes: new opportunities and practical applications. John Wiley & Sons; 2016 Aug 22.

[62] Li P, Wang Z, Qiao Z, Liu Y, Cao X, Li W, Wang J, Wang S. Recent developments in membranes for efficient hydrogen purification. Journal of Membrane Science. 2015 Dec 1;495:130-68.

[63] Hwa LC, Rajoo S, Noor AM, Ahmad N, Uday MB. Recent advances in 3D printing of porous ceramics: A review. Current Opinion in Solid State and Materials Science. 2017 Dec 1;21(6):323-47.

[64] Wu C, Luo Y, Cuniberti G, Xiao Y, Gelinsky M. Three-dimensional printing of hierarchical and tough mesoporous bioactive glass scaffolds with a controllable pore architecture, excellent mechanical strength and mineralization ability. Acta biomaterialia. 2011 Jun 1;7(6):2644-50.

[65] Griffith ML, Halloran JW. Freeform fabrication of ceramics via stereolithography; 1996.

[66] Aleni AH, Kretzschmar N, Jansson A, Ituarte IF, St-Pierre L. 3D printing of dense and porous TiO2 structures. Ceramics International. 2020 Apr 1.

[67] Maurath J, Willenbacher N. 3D printing of open-porous cellular ceramics with high specific strength. Journal of the European Ceramic Society. 2017 Dec 1;37(15):4833-42.

[68] Minas C, Carnelli D, Tervoort E, Studart AR. 3D printing of emulsions and foams into hierarchical porous ceramics. Advanced Materials. 2016 Dec;28(45):9993-9.

[69] Moon YW, Choi IJ, Koh YH, Kim HE. Porous alumina ceramic scaffolds with biomimetic macro/micro-porous structure using three-dimensional (3-D) ceramic/camphene-based extrusion. Ceramics International. 2015 Nov 1;41(9):12371-7.

[70] Chang CH, Lin CY, Liu FH, Chen MH, Lin CP, Ho HN, Liao YS. 3D printing bioceramic porous scaffolds with good mechanical property and cell affinity. PloS one. 2015 Nov 30;10(11):e0143713.

[71] Fielding G, Bose S. SiO2 and ZnO dopants in three-dimensionally printed tricalcium phosphate bone tissue engineering scaffolds enhance osteogenesis and angiogenesis in vivo. Acta biomaterialia. 2013 Nov 1;9(11):9137-48.

[72] Kothari VK, Das A, Singh S. Filtration behaviour of woven and nonwoven fabrics. 2007.

[73] Fogliatto AA, Ahrens CH, Wendhausen PA, Santos EC, Rodrigues D. Correlation between porosity and permeability of stainless steel filters with gradient porosity produced by SLS/SLM. Rapid Prototyping Journal. 2019 Aug 9.

[74] Kale AB, Kim BK, Kim DI, Castle EG, Reece M, Choi SH. An investigation of the corrosion behavior of 316L stainless steel fabricated by SLM and SPS techniques. Materials Characterization. 2020 May 1;163:110204.

[75] Yadroitsev I, Shishkovsky I, Bertrand P, Smurov I. Manufacturing of fine-structured 3D porous filter elements by selective laser melting. Applied Surface Science. 2009 Mar 1;255(10):5523-7.

[76] Imwinkelried T. Mechanical properties of open-pore titanium foam. Journal of biomedical materials research Part A. 2007 Jun 15;81(4):964-70.

[77] Heinl P, Müller L, Körner C, Singer RF, Müller FA. Cellular Ti–6Al–4V structures with interconnected macro porosity for bone implants fabricated by selective electron beam melting. Acta biomaterialia. 2008 Sep 1;4(5):1536-44.

[78] Dong Y, Lin B, Zhou JE, Zhang X, Ling Y, Liu X, Meng G, Hampshire S. Corrosion resistance characterization of porous alumina membrane supports. Materials Characterization. 2011 Apr 1;62(4):409-18.

[79] Chun YS, Kim YW. Processing and mechanical properties of porous silica-bonded silicon carbide ceramics. Metals and materials International. 2005 Oct 1;11(5):351-5.

[80] Fukasawa T, Deng ZY, Ando M, Ohji T, Kanzaki S. Synthesis of porous silicon nitride with unidirectionally aligned channels using freeze-drying process. Journal of the American Ceramic Society. 2002 Sep;85(9):2151-5.

[81] Yu F, Xie H, Bai Y, Xu F, Han P, Tian L, Ni S. Synthesis of porous silicon nitride with unidirectionally aligned channels using extrusion method. Ceramics–Silikáty. 2018 Aug 1;62(3):248-52.

[82] Fane AG, An J, Chua CK, Chong TH, Tan WS. Selective Laser Sintering Of Polypropylene Feed Spacers For Spiral Wound Membrane Modules.

[83] Thomas N, Sreedhar N, Al-Ketan O, Rowshan R, Al-Rub RK, Arafat H. 3D printed triply periodic minimal surfaces as spacers for enhanced heat and mass transfer in membrane distillation. Desalination. 2018 Oct 1;443:256-71.

[84] Thomas N, Sreedhar N, Al-Ketan O, Rowshan R, Al-Rub RK, Arafat H. 3D printed spacers based on TPMS architectures for scaling control in membrane distillation. Journal of Membrane Science. 2019 Jul 1;581:38-49.

[85] Yanar N, Son M, Yang E, Kim Y, Park H, Nam SE, Choi H. Investigation of the performance behavior of a forward osmosis membrane system using various feed spacer materials fabricated by 3D printing technique. Chemosphere. 2018 Jul 1;202:708-15.

[86] Veiga AR, Calmanovici CE, Giulietti M. Operational conditions evaluation in ammonium bicarbonate crystallization. In Proceedings of the 14th International Symposium on Industrial Crystallization 1999 (Vol. 65, pp. 1-12).

[87] Kurgan N. Effect of porosity and density on the mechanical and microstructural properties of sintered 316L stainless steel implant materials. Materials & Design. 2014 Mar 1;55:235-41.

[88] Dalwadi MP, Griffiths IM, Bruna M. Understanding how porosity gradients can make a better filter using homogenization theory. Proceedings of the Royal Society A: Mathematical, Physical and Engineering Sciences. 2015 Oct 8;471(2182):20150464.

[89] Solakoğlu EU, Yilmaz R, Oren S, Akbulut G, Poyraz O, Yasa E. Process limits of direct metal laser sintering (dmls) in terms of minimum hole and boss diameters with varying aspect ratios.

[90] Bertoli US, MacDonald BE, Schoenung JM. Stability of cellular microstructure in laser powder bed fusion of 316L stainless steel. Materials Science and Engineering: A. 2019 Jan 2;739:109-17.

[91] Wang D, Song C, Yang Y, Bai Y. Investigation of crystal growth mechanism during selective laser melting and mechanical property characterization of 316L stainless steel parts. Materials & Design. 2016 Jun 15;100:291-9.

[92] Cherry JA, Davies HM, Mehmood S, Lavery NP, Brown SG, Sienz J. Investigation into the effect of process parameters on microstructural and physical properties of 316L stainless steel parts by selective laser melting. The International Journal of Advanced Manufacturing Technology. 2015 Feb 1;76(5-8):869-79.

[93] Sun Z, Tan X, Tor SB, Yeong WY. Selective laser melting of stainless steel 316L with low porosity and high build rates. Materials & Design. 2016 Aug 15;104:197-204.